Steel and Composite Structures, *Vol. 29, No. 6 (2018) 781-798*
DOI: https://doi.org/10.12989/scs.2018.29.6.781

Ultimate strength estimation of composite plates under combined in-plane and lateral pressure loads using two different numerical methods

S.A.M. Ghannadpour *, M. Shakeri and A. Kurkaani Barvaj

Aerospace Engineering Department, Faculty of New Technologies and Engineering, Shahid Beheshti University, G.C, Tehran, Iran

(*Received September 19, 2018, Revised October 12, 2018, Accepted December 31, 2018*)

Abstract. In this paper, two different computational methods, called Rayleigh-Ritz and collocation are developed to estimate the ultimate strength of composite plates. Progressive damage behavior of moderately thick composite laminated plates is studied under in-plane compressive load and uniform lateral pressure. The formulations of both methods are based on the concept of the principle of minimum potential energy. First order shear deformation theory and the assumption of large deflections are used to develop the equilibrium equations of laminated plates. Therefore, Newton-Raphson technique will be used to solve the obtained system of nonlinear algebraic equations. In Rayleigh-Ritz method, two degradation models called complete and region degradation models are used to estimate the degradation zone around the failure location. In the second method, a new energy based collocation technique is introduced in which the domain of the plate is discretized into the Legendre-Gauss-Lobatto points. In this new method, in addition to the two previous models, the new model named node degradation model will also be used in which the material properties of the area just around the failed node are reduced. To predict the failure location, Hashin failure criteria have been used and the corresponding material properties of the failed zone are reduced instantaneously. Approximation of the displacement fields is performed by suitable harmonic functions in the Rayleigh-Ritz method and by Legendre basis functions (LBFs) in the second method. Finally, the results will be calculated and discussions will be conducted on the methods.

Keywords: ultimate strength; Hashin failure criteria; collocation; Rayleigh-Ritz; composite plate; Legendre-Gauss-Lobatto nodes; geometric nonlinear analysis

1. Introduction

Fiber reinforced composite materials have increasingly used to improve the structural efficiency in many engineering fields. Composite plates have been widely used in various industries such as spacecraft, marine, and automobiles because of their advantages of weight and mechanical properties with a comparison to the metallic structures. Various types of failure and damage may occur in these structures that have been extensively studied in recent decades (Jin and Batra 1999, Tornabene *et al*. 2018, Kamareh *et al*. 2018). Due to the variety of their applications, composite plates are subjected to different loading conditions. In this paper, the composite laminated plates are considered to be under in-plane compressive loads and lateral pressure loads. In this situation, buckling, post-buckling and nonlinear phenomena for these structures should also be discussed. Therefore, the main subject of this paper is the evaluation of the ultimate strength and damage prediction of composite plates under combined in-plane compressive loads and lateral pressure loads.

Before starting the research, it is necessary to give a brief overview of past research. A lot of research has been done on static, buckling, post-buckling and geometric nonlinear analyses of plates and plate structures. Static analysis of inter-laminar stresses and free edge effects in a laminated composite beam resting on the Winkler-type elastic foundation has been discussed by Afshin and Taheri-Behrooz (2015) using Reddy's layerwise theory. In the research published by Argyris and Tenek (1997), complete reviews on studies of buckling and post-buckling of structures by different methods have been reported. Batra and Xiao (2013) studied the post-buckling and delamination analyses of straight and curved laminated beams using a layer-wise third order theory incorporating a cohesive zone model. The applicability of a new extended layerwise approach for thermal buckling load optimization of laminated plates has been investigated by Topal (2013). Patel (2014) studied nonlinear bending of composite stiffened plates subjected to uniform transverse loading. Dynamic behavior of FGM plates with different edge boundary condition has been discussed by Chakraverty and Pradhan (2014). Paik *et al*. (2015) investigated the localization of buckling modes in plates and laminates using Mindlin plate theory and the finite element method. Becheri *et al*. (2016) investigated the buckling of symmetrically composite plates due to n^{th}-order shear deformation theory with curvature effect by an exact analytical solution. Buckling and post-buckling thermo-mechanical deformations of an FGM Timoshenko beam are also investigated by Sun *et al*. (2016). In another study, Jiang

*Corresponding author, Ph.D.,
E-mail: a_ghannadpour@sbu.ac.ir

ISSN: 1229-9367 (Print), 1598-6233 (Online)

et al. (2018) investigated thermal effects on the buckling, post-buckling and nonlinear vibration behaviors of composite laminated trapezoidal plates. In recent years, many studies have been conducted on laminated composite arbitrarily shaped plates. For example, Fantuzzi and Tornabene (2016) developed a strong form collocation method for solving laminated composite plates wherein discontinuities arise. They used the Differential Quadrature (DQ) method for solving the mathematical problem and isogeometric mapping was implemented for the nonlinear mapping of complex shapes. In another similar research, Fantuzzi *et al*. (2018) developed the strong formulation finite element method and the weak form was solved using commercial fin2ite element packages based on the domain decomposition technique according to geometric discontinuities.

The finite element method (FEM) is although one of the most practical and commonly used methods for analyzing the buckling and post-buckling behaviors of plates, it requires a large number of degrees of freedom to obtain acceptable results and therefore extremely large data and computer core is needed. Zhang and Yang (2009) presented recent developments in finite element analysis for laminated composite plates. As an alternative method for analyzing the buckling and post-buckling of composite plates and plate structures, the finite strip method (FSM) may be used which is based on the discretization of the domain into longitudinal strips. Buckling and post-buckling of relatively thick and symmetrically cross-ply laminates using exact finite strip method have been investigated by Ghannadpour *et al*. (2014). The post-buckling behavior of functionally graded plates in thermal environments using semi-analytical finite strip method has also studied by Ovesy *et al*. (2015). The post-buckling response and nonlinear behavior of imperfect composite plates, when subjected to progressive end-shortening has been predicted by Ovesy *et al*. (2005) using two different versions of the finite strip method. Ghannadpour and Ovesy (2009a) analyzed the buckling of laminated composite plates and prismatic plate structures using exact finite strip method. They have also studied the buckling and initial post-buckling analyzes of channel section and Box section struts using an exact finite strip (Ghannadpour and Ovesy 2009b, Ovesy and Ghannadpour 2011). It can be seen in the literature that other numerical and computational techniques have also been used for buckling and post-buckling analyzes of plate structures. One of the most commonly used methods is the meshless or mesh-free methods. Naghsh *et al*. (2018) focused on analyzing the thermal buckling point-supported thin laminated composite plates by the element-free Galerkin method. Recently, Vu *et al*. (2018) have presented a novel mesh-free method for investigating the buckling, bending and free vibration behavior of FGM plates. Ghannadpour and Kiani (2018) investigated the post-buckling and geometrically nonlinear behaviors of imperfect functionally graded plates using spectral collocation method. More recently, Ghannadpour and Mehrparvar have investigated the post-buckling and nonlinear behaviors of relatively thick composite and functionally graded plates containing elliptical and rectangular cutouts using two new computational approaches (Ghannadpour and Mehrparvar 2018, Mehrparvar and Ghannadpour 2018).

In all previously mentioned works, linear and nonlinear behaviors of composite plates have been investigated without considering the effects of damage and failure. Since the main purpose of this study is to examine both analyzes of geometric nonlinearity and progressive damage of composite plates, therefore it is also necessary to give a brief review about fracture, damage and ultimate strength of composite plates. It should be noted that the ultimate strength analyzes of composite plates are usually conducted by the finite element method. A brief review of studies of fracture and damage of composite laminates can be found in the paper published by Vedrtnam and Pawar (2017). Progressive damage modeling of open-hole composite laminates has been investigated by Su *et al*. (2015). They have used the finite element method and for failure analysis, the quadratic Hashin failure criteria have been used. In another finite element research work, Muthusamy and Sivakumar (2014) have predicted the onset and the progression of damage in the continuous fiber reinforced composite laminates taking into consideration the different mechanical behavior of the constituents in the composites under different loading conditions. Aghaei *et al*. (2015) investigated damage analysis of composite beams subjected to low velocity impact by different failure criteria implemented in ABAQUS software. A finite-element model for composite beams with partially delaminated layers has been used by Mahieddinet *et al*. (2015) to investigate their behavior. In their formulation account was taken of lateral strains and the first-order shear deformation theory was used.

It should be noted that if a damage research was carried out by the finite element method, it is a very complex and high time-consuming procedure. Simplified and reliable methods for such analyzes are required that could easily and quickly be used to estimate the ultimate strength of composite plates. Tornabene *et al*. (2017) proposed a mathematical scheme to model a damaged mechanical configuration for laminated plates and shells. Their theoretical framework for the two-dimensional shell model was based on a unified formulation able to study and compare several Higher-order Shear Deformation Theories (HSDTs). To analyze the buckling and ultimate strength of metal plates with and without stiffener, a group of simplified methods has been developed by Brubak *et al*. (2007) and by Brubak and Hellesland (2007a, 2007b, 2008). Recently, analysis of ultimate strength of imperfect composite plates has been carried out by Hayman *et al*. (2011). This study includes simply supported square laminated composite plates under in-plane loads that their results were validated with finite element analysis. The calculation of the first ply failure load and ultimate strength of imperfect simply-supported composite plates under in-plane compressive load and with the assumptions of small deflection theory have been done by Yang *et al*. (2013). They have used the well-known Ritz method based on the first order shear deformation theory. The degradation model in their analysis was instantaneous material degradation that applied in complete ply or region of failed ply. A similar

study but with the assumptions of large deflection theory has also been reported by Yang and Hayman (2015a). In their recent research (2015a), they have also investigated the ultimate strength and geometric nonlinear behavior of imperfect simply-supported composite plates with linear material degradation model. More recently, Ghannadpour and Shakeri (2018) presented energy based collocation method to progressive damage analysis of composite plates under compressive loads. In their analysis, nonlinear terms in the strain-displacement relations were neglected. In the latest research, Ghannadpour *et al*. (2018) studied the geometric nonlinear and progressive damage behavior of relatively thick and simply supported composite plates subjected to end-shortening and uniform and sinusoidal lateral pressure loads using Ritz approach.

With the above descriptions, in this paper, ultimate strength, post-buckling and geometric nonlinear analyzes of composite plates have been investigated using two different numerical methods. The plates are considered to be subjected to both in-plane compressive and lateral pressure loads. Moderately thick laminates have been analyzed and therefore first order shear deformation plate theory is considered with the assumptions of large deflections. The square plates with all simply-supported edges and also plates with some clamped edges are considered in this study. The in-plane boundary conditions are chosen in such a way that all four edges of the plates are kept straight. As mentioned before, two different numerical methods, called Rayleigh-Ritz and collocation are introduced to estimate the ultimate strength of composite plates. The formulations of two methods are based on the concept of the principle of minimum potential energy and Newton–Raphson technique will be used to solve the obtained system of nonlinear algebraic equations. In the Rayleigh-Ritz method, two degradation models have been used with material degradation either applied to the entire failed ply that is called complete degradation model (CDM) or to the affected regions of a failed ply called region degradation model (RDM). In the second method, a new energy based collocation technique is introduced in which the domain of the plate is discretized into the Legendre-Gauss-Lobatto points. In this method, in addition to the two previous models (i.e. CDM and RDM), the new model named node degradation model (NDM) will also be used in which the material properties of the area just around the failed node are reduced. To predict the failure location in both methods, Hashin failure criteria have been used and the corresponding material properties of the failed zone are reduced instantaneously.

2. Theoretical development

2.1 Basic formulations

A rectangular laminated plate of dimensions of $a \times b$ and the total thickness h is considered. The origin of the coordinate is assumed to be located at the center of the plate. The laminate is considered to be subjected to in-plane compressive loads on the edge $x = a/2$ along the x-direction called N_x and uniform lateral pressure loads on the plate along the z-direction. Two different types of boundary conditions are considered that they will be presented in details in the next section. The laminates are assumed to be moderately thick, thus theoretical formulations are based on the first order shear deformation theory (FSDT). With that, the displacements in the plate can be described by the following relations줌

$$d_x(x,y,z) = u(x,y) + z\varphi_x \tag{1a}$$

$$d_y(x,y,z) = v(x,y) + z\varphi_y \tag{1b}$$

$$d_z(x,y,z) = w(x,y) \tag{1c}$$

Where (u, v, w) are displacements of mid-plane, and φ_x and φ_y denote the rotations of a transverse normal about axes parallel to the y and x axes, respectively. Therefore, the deformation of a laminated plate is expressed by

$$\mathbb{d} = \boldsymbol{u} + \mathrm{z}\boldsymbol{\vartheta} \tag{2}$$

Where $\mathbb{d} = \langle d_x \quad d_y \quad d_z \rangle^T$ is called the displacement vector and $\boldsymbol{u} = \langle u \quad v \quad w \rangle^T$ and $\boldsymbol{\vartheta} = \langle \varphi_x \quad \varphi_y \quad 0 \rangle^T$ are mid-plane displacement and rotation vectors, respectively.

The vector of strains $\boldsymbol{e}$ with the assumptions of moderately large displacements is written as

$$\boldsymbol{e} = \langle e_{xx} \quad e_{yy} \quad e_{xy} \quad e_{xz} \quad e_{yz} \quad e_{zz} \rangle^T = \begin{Bmatrix} \boldsymbol{e}_p \\ \boldsymbol{e}_n \end{Bmatrix} \tag{3}$$

Where $\boldsymbol{e}_p$ and $\boldsymbol{e}_n$ denote the in-plane and out-of-plane components vectors with subscripts p and n, respectively. By considering the geometric nonlinearity, the strain-displacement relations can be given as

$$\begin{aligned} \boldsymbol{e}_p &= \boldsymbol{\mathcal{D}}_p \boldsymbol{u} + \frac{1}{2}\left(\boldsymbol{\mathcal{D}}_p \otimes w\right)\boldsymbol{\mathcal{D}}_n \boldsymbol{u} + z\,\boldsymbol{\mathcal{D}}_p \boldsymbol{\vartheta} \\ &= \boldsymbol{\varepsilon}_p + \boldsymbol{\varepsilon}_{nl} + z\boldsymbol{\kappa} = \boldsymbol{\varepsilon}_0 + z\boldsymbol{\kappa} \end{aligned} \tag{4a}$$

$$\boldsymbol{e}_n = \boldsymbol{\mathcal{D}}_n \boldsymbol{u} + \boldsymbol{\vartheta} = \boldsymbol{\gamma} \tag{4b}$$

Where $\otimes$ denotes the Kronecker product. Also Eqs. (4) define the plate strain vectors that are the in-plane strains vector $\boldsymbol{\varepsilon}_0$, the curvatures vector $\boldsymbol{\kappa}$, and the shear strains vector $\boldsymbol{\gamma}$. In writing the above equations, two operators $\boldsymbol{\mathcal{D}}_p$ and $\boldsymbol{\mathcal{D}}_n$ have been used which are defined as follows

$$\boldsymbol{\mathcal{D}}_p = \begin{bmatrix} \dfrac{\partial}{\partial x} & 0 & 0 \\ 0 & \dfrac{\partial}{\partial y} & 0 \\ \dfrac{\partial}{\partial y} & \dfrac{\partial}{\partial x} & 0 \end{bmatrix}; \quad \boldsymbol{\mathcal{D}}_n = \begin{bmatrix} 0 & 0 & \dfrac{\partial}{\partial x} \\ 0 & 0 & \dfrac{\partial}{\partial y} \\ 0 & 0 & 0 \end{bmatrix} \tag{5}$$

To describe the mechanical state, the stress vector $\boldsymbol{\sigma}$ is defined as

$$\boldsymbol{\sigma} = \langle \sigma_{xx} \quad \sigma_{yy} \quad \sigma_{xy} \quad \sigma_{xz} \quad \sigma_{yz} \quad \sigma_{zz} \rangle^T = \begin{Bmatrix} \boldsymbol{\sigma}_p \\ \boldsymbol{\sigma}_n \end{Bmatrix} \tag{6}$$

The constitutive equations for the oriented k^{th} orthotropic ply of the laminate with the assumption that the

plate is in a state of plane stress ($\sigma_{zz}=0$) are

$$\boldsymbol{\sigma}_p^{(k)}=\bar{\boldsymbol{Q}}_p^{(k)}\boldsymbol{e}_p;\ \bar{\boldsymbol{Q}}_p^{(k)}=\begin{bmatrix}\bar{Q}_{11} & \bar{Q}_{12} & \bar{Q}_{16}\\ \bar{Q}_{12} & \bar{Q}_{22} & \bar{Q}_{26}\\ \bar{Q}_{16} & \bar{Q}_{26} & \bar{Q}_{66}\end{bmatrix}^{(k)} \tag{7a}$$

$$\boldsymbol{\sigma}_n^{(k)}=\bar{\boldsymbol{Q}}_n^{(k)}\boldsymbol{e}_n;\ \bar{\boldsymbol{Q}}_n^{(k)}=\begin{bmatrix}\bar{Q}_{55} & \bar{Q}_{45} & 0\\ \bar{Q}_{45} & \bar{Q}_{44} & 0\\ 0 & 0 & 0\end{bmatrix}^{(k)} \tag{7b}$$

The internal forces and moments which are measured per unit length are including, the in-plane stress resultants $\boldsymbol{N}$, the moment resultants $\boldsymbol{M}$ and the transverse force resultants $\boldsymbol{T}$ and they can be obtained by

$$\begin{Bmatrix}\boldsymbol{N}\\ \boldsymbol{M}\\ \boldsymbol{T}\end{Bmatrix}=\begin{bmatrix}\boldsymbol{A}_p & \boldsymbol{B} & 0\\ \boldsymbol{B} & \boldsymbol{D} & 0\\ 0 & 0 & \boldsymbol{A}_n\end{bmatrix}\begin{Bmatrix}\boldsymbol{\varepsilon}_0\\ \boldsymbol{\kappa}\\ \boldsymbol{\gamma}\end{Bmatrix}=\boldsymbol{S\varepsilon} \tag{8}$$

In which $\boldsymbol{A}_p$, $\boldsymbol{B}$, $\boldsymbol{D}$,and $\boldsymbol{A}_n$ are the generalized stiffness matrices, which are extensional stiffness matrix, extensional-bending stiffness matrix, bending stiffness and interlaminar shear stiffness matrices, respectively. They can be computed by the following equations.

$$\left(\boldsymbol{A}_p,\boldsymbol{B},\boldsymbol{D}\right)=\sum_{k=1}^{N_\ell}\int_{h_{k-1}}^{h_k}\bar{\boldsymbol{Q}}_p^{(k)}(1,z,z^2)\,dz \tag{9a}$$

$$\boldsymbol{A}_n=K\sum_{k=1}^{N_\ell}\int_{h_{k-1}}^{h_k}\bar{\boldsymbol{Q}}_n^{(k)}\,dz \tag{9b}$$

Where K is the shear correction factor. The total potential energy Π for a laminated plate is consists of the strain energy of the plate $\mathcal{U}$ and potential energy of external forces $\mathcal{V}$. The strain energy of the plate $\mathcal{U}$ can be obtained by the following relation.

$$\begin{aligned}\mathcal{U}&=\frac{1}{2}\iiint_V\boldsymbol{\sigma}^T\boldsymbol{e}\,dV=\frac{1}{2}\iint_\Omega\int_z\boldsymbol{\sigma}^T\boldsymbol{e}\,dzd\Omega\\&=\frac{1}{2}\iint_\Omega\boldsymbol{\varepsilon}^T\boldsymbol{S\varepsilon}\,d\Omega\end{aligned} \tag{10}$$

Where Ω is the domain occupied by the plate mid-plane. Since in the current study, the laminates are subjected to in-plane compressive loads and also uniform lateral pressure load, the potential energy of external forces and loads can be computed by introducing the external force vector $\widetilde{\boldsymbol{\mathcal{F}}}=\langle N_x\quad N_y\quad N_{xy}\rangle^T$ and also pressure vector $\widetilde{\boldsymbol{\mathcal{P}}}=\langle 0\quad 0\quad P_0\rangle^T$. Parameter P_0 denote the uniform pressure value that is applied to the whole plate in the z-direction. Therefore, the potential energy of external forces $\mathcal{V}$ and finally the total potential energy of a laminate can be obtained by

$$\mathcal{V}=-\iint_\Omega\left(\boldsymbol{\varepsilon}_p^T\widetilde{\boldsymbol{\mathcal{F}}}-\boldsymbol{u}^T\widetilde{\boldsymbol{\mathcal{P}}}\right)d\Omega \tag{11a}$$

$$\Pi=\mathcal{U}+\mathcal{V} \tag{11b}$$

By using Eqs. (4)-(9)-(10) and (11), the total potential energy Π can finally be written as follows

$$\begin{aligned}\Pi=\frac{1}{2}\iint_\Omega\big(&\boldsymbol{\varepsilon}_0^T\boldsymbol{A}_p\boldsymbol{\varepsilon}_0+\boldsymbol{\varepsilon}_0^T\boldsymbol{B\kappa}+\boldsymbol{\kappa}^T\boldsymbol{B\varepsilon}_0\\&+\boldsymbol{\kappa}^T\boldsymbol{D\kappa}+\boldsymbol{\gamma}^T\boldsymbol{A}_n\boldsymbol{\gamma}-2\boldsymbol{\varepsilon}_p^T\widetilde{\boldsymbol{\mathcal{F}}}+2\boldsymbol{u}^T\widetilde{\boldsymbol{\mathcal{P}}}\big)d\Omega\end{aligned} \tag{12}$$

2.2 Boundary conditions

In order to calculate the total potential energy of a laminate, it is required to approximate the displacement fields of the problem. In order to approximate the displacement functions, it is necessary to describe the essential boundary conditions. Two different types of boundary conditions are considered in this study; the square plates with simply supported on all edges (type A) and the square plates with clamped edges in the y-direction and simply supported edges in the x-direction (type B). The plate is assumed to be under in-plane compressive loads on the edge $x=a/2$ along the x-direction and as mentioned earlier it is subjected to lateral pressure loads on the plate along the z-direction.

For in-plane boundary conditions, all edges of the plate are kept straight for any in-plane movement and therefore u_c and v_c which are shown in Fig. 1 are for satisfying these straight conditions. As it can be seen, the labelling schemes are included in these figures to assign the related boundary conditions. The letter *S* refers to simply supported boundary condition and the letter *C* refers to clamped boundary condition on the specified edge. Therefore, based on mentioned conditions, the two aforementioned boundary conditions are different from the viewpoint of out-of-plane boundary conditions.

Since the problem-solving technique in this study is based on minimizing the total potential energy functional, the approximated displacement fields have to satisfy only the essential boundary conditions.

3. Equilibrium equations and solution procedure in Rayleigh-Ritz method

In the Rayleigh-Ritz method employed in this research, the displacement fields of the problem are approximated by harmonic functions. Given the boundary conditions in the previous section, the required displacement fields for type A boundary conditions are

$$\varphi_x(\bar{x},\bar{y})=\sum_{i=1}^{N_t^R}\sum_{j=1}^{N_t^R}R_{ij}^{\varphi_x}\cos\left(i\pi\frac{(\bar{x}+1)}{2}\right)\sin\left(j\pi\frac{(\bar{y}+1)}{2}\right) \tag{13a}$$

$$\varphi_y(\bar{x},\bar{y})=\sum_{i=1}^{N_t^R}\sum_{j=1}^{N_t^R}R_{ij}^{\varphi_y}\sin\left(i\pi\frac{(\bar{x}+1)}{2}\right)\cos\left(j\pi\frac{(\bar{y}+1)}{2}\right) \tag{13b}$$

$$w(\bar{x},\bar{y})=\sum_{i=1}^{N_t^R}\sum_{j=1}^{N_t^R}R_{ij}^{w}\sin\left(i\pi\frac{(\bar{x}+1)}{2}\right)\sin\left(j\pi\frac{(\bar{y}+1)}{2}\right) \tag{13c}$$

$$u(\bar{x},\bar{y}) = \sum_{i=1}^{N_t^R}\sum_{j=1}^{N_t^R} R_{ij}^{u} \sin\left(i\pi\frac{(\bar{x}+1)}{2}\right)\sin\left(j\pi\frac{(\bar{y}+1)}{2}\right) + \frac{u_c(\bar{x}+1)}{2} \quad (13d)$$

$$v(\bar{x},\bar{y}) = \sum_{i=1}^{N_t^R}\sum_{j=1}^{N_t^R} R_{ij}^{v} \sin\left(i\pi\frac{(\bar{x}+1)}{2}\right)\sin\left(j\pi\frac{(\bar{y}+1)}{2}\right) + \frac{v_c(\bar{y}+1)}{2} \quad (13e)$$

For type B, all displacement fields are similar to type A except the displacement fields φ_y and w that can be defined as

$$\varphi_y(\bar{x},\bar{y}) = \sum_{i=1}^{N_t^R}\sum_{j=1}^{N_t^R} R_{ij}^{\varphi_y} \sin\left(i\pi\frac{(\bar{x}+1)}{2}\right)\sin\left(j\pi\frac{(\bar{y}+1)}{2}\right) \quad (13f)$$

$$w(\bar{x},\bar{y}) = \sum_{i=1}^{N_t^R}\sum_{j=1}^{N_t^R} R_{ij}^{w} \sin\left(i\pi\frac{(\bar{x}+1)}{2}\right)\sin^2\left(j\pi\frac{(\bar{y}+1)}{2}\right) \quad (13g)$$

Where $\bar{x}$ and $\bar{y}$ are non-dimensional coordinates defined as $2x/a$ and $2y/b$, respectively and N_t^R is the number of terms in the series expansion which is taken same for all displacement fields. The coefficients u_c, v_c and R_{ij}^{τ} where $\tau \in \{u, v, w, \varphi_x, \varphi_y\}$ are unknowns of the problem in the Rayleigh-Ritz method that should be found, and parameters i and j are positive integers. The coefficients u_c, v_c are for satisfying the straight conditions mentioned in Fig. 1 for in-plane displacements (u, v).

The total potential energy can ultimately be rewritten in a matrix form by using the Hessian technique.

$$\Pi = -\boldsymbol{d}^T\boldsymbol{V}_F + \frac{1}{2}\boldsymbol{d}^T\boldsymbol{K}_0\boldsymbol{d} + \frac{1}{6}\boldsymbol{d}^T\boldsymbol{K}_1(\boldsymbol{d})\boldsymbol{d} + \frac{1}{12}\boldsymbol{d}^T\boldsymbol{K}_2(\boldsymbol{d})\boldsymbol{d} \quad (14)$$

Where $\boldsymbol{V}_F$ is a column matrix of constants including the effects of applied loads. The column matrix $\boldsymbol{d}$ contains the unknown of the problems. Subscript 0 is for symmetric square stiffness matrices whose coefficients are constant whilst subscript 1 and 2 are for matrices with linear and quadratic functions of the unknowns, respectively. The unknown coefficients of the problem are found by solving the nonlinear equilibrium equations which can be obtained by the application of the principle of minimum potential energy as

$$\boldsymbol{F}(\boldsymbol{d}) = -\boldsymbol{V}_F + \left(\boldsymbol{K}_0 + \frac{1}{2}\boldsymbol{K}_1(\boldsymbol{d}) + \frac{1}{3}\boldsymbol{K}_2(\boldsymbol{d})\right)\boldsymbol{d} = \boldsymbol{0} \quad (15)$$

To solve the above nonlinear algebraic equations, the well-known Newton–Raphson technique is used. To do that, a vector $\boldsymbol{d_i}$ is assumed as an approximate trial solution at a particular force $N$and load P_0. $\boldsymbol{F}(\boldsymbol{d_i})$ indicates the error equations for the approximation. By applying the Newton-Raphson process, an improved solution $\boldsymbol{d_{i+1}}$ is found by equating to zero the curtailed Taylor's expansion of $\boldsymbol{F}(\boldsymbol{d_{i+1}})$ in the neighbourhood of $\boldsymbol{d_i}$ as

$$\boldsymbol{F}(\boldsymbol{d_{i+1}}) \simeq \boldsymbol{F}(\boldsymbol{d_i}) + \frac{\partial \boldsymbol{F}(\boldsymbol{d_i})}{\partial \boldsymbol{d_i}}(\boldsymbol{d_{i+1}} - \boldsymbol{d_i}) = 0$$
$$\boldsymbol{F}(\boldsymbol{d_i}) + \{\boldsymbol{K}_0 + \boldsymbol{K}_1(\boldsymbol{d_i}) + \boldsymbol{K}_2(\boldsymbol{d_i})\}(\boldsymbol{d_{i+1}} - \boldsymbol{d_i}) = 0 \quad (16)$$

In order to obtain the accurate results, the relevant convergence criteria are defined based on both the vector containing the unknown coefficients $(\boldsymbol{d})$ and all equations containing these coefficients i.e., $\boldsymbol{F}(\boldsymbol{d})$. The iterative procedure is repeated until the following conditions including convergence of the solution vector and satisfaction of the equations are satisfied concurrently.

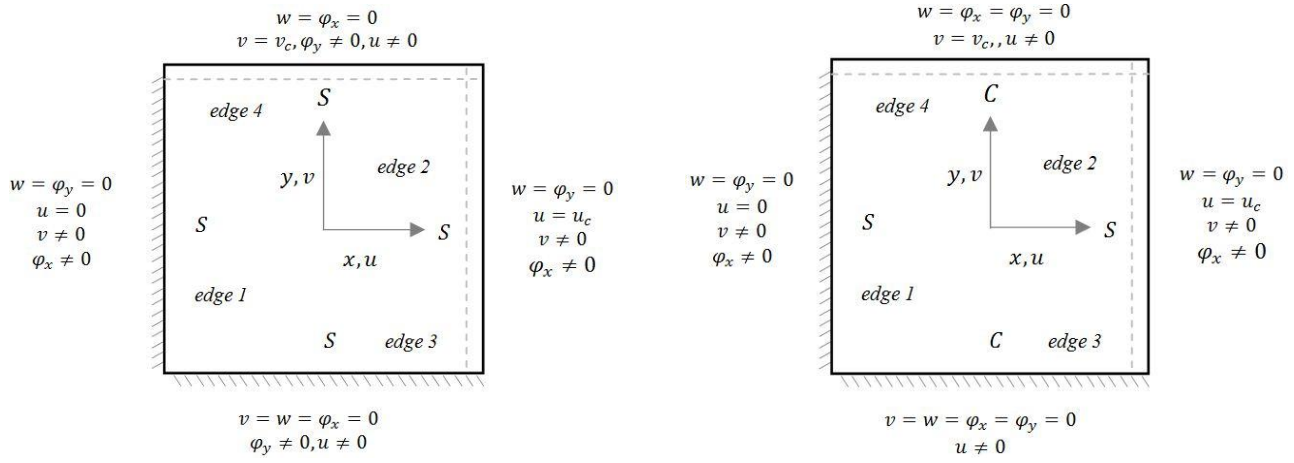

Fig. 1 Boundary conditions type A (a) and type B (b)

$$\frac{\|\Delta \boldsymbol{d}_r\|}{\|\boldsymbol{d}_{r+1}\|} < 5\times 10^{-5} \\ \|\boldsymbol{F}(\boldsymbol{d}_r)\| < 5\times 10^{-5} \tag{17}$$

where r is the iteration counter in Newton-Raphson technique and $\|.\|$ denotes the 2-norm.

4. Equilibrium equations and solution procedure in collocation method

In the collocation method, the approximation of displacement fields is performed by Legendre basis functions P which is one of the most powerful mathematical series for numerical methods. Legendre basis functions or Legendre polynomials are solutions to the following Legendre differential equation

$$\frac{d}{dx}\left[(1-x^2)\frac{d}{dx}P_n(x)\right] + n(n+1)P_n(x) = 0 \tag{18}$$

Also, Legendre polynomials satisfy the three-term recursion as

$$P_{n+1}(x) = \frac{2n+1}{n+1}xP_n(x) - \frac{n}{n+1}P_{n-1}(x) \tag{19}$$

Where $P_0(x)=1$ and $P_1(x)=x$. Therefore, the displacement fields of the problem can be approximated by the following relations.

$$\tau\,(\bar{x},\bar{y}) = \mathbb{B}_\tau(\bar{x},\bar{y})\sum_{i=1}^{N_t^C}\sum_{j=1}^{N_t^C} C_{ij}^\tau P_{i-1}(\bar{x})P_{j-1}(\bar{y}) \\ +f_\tau(\bar{x},\bar{y})C_c^\tau = \boldsymbol{\mathcal{T}}_\tau^T\boldsymbol{\mathcal{C}}_\tau \tag{20}$$

Where $\tau \in \{u,v,w,\varphi_x,\varphi_y\}$ is a displacement field and N_t^C is the number of terms in the series expansion which is taken same for all displacement fields as before method. The coefficients C_{ij}^τ and C_c^τ (i.e., $C_c^u \equiv u_c$ and $C_c^v \equiv v_c$) are the unknown coefficients in the collocation method and function $f_\tau(\bar{x},\bar{y})$ is defined as below

$$f_\tau(\bar{x},\bar{y}) = \begin{cases}(1+\bar{x})/2 & \text{for } \tau \equiv u\\ (1+\bar{y})/2 & \text{for } \tau \equiv v\\ 0 & \forall\,\tau\in\{w,\varphi_x,\varphi_y\}\end{cases} \tag{21}$$

The so-called boundary function $\mathbb{B}_\tau(\bar{x},\bar{y})$ is also chosen to ensure the fulfillment of the essential boundary conditions mentioned in Fig. 1. It can be defined as

$$\mathbb{B}_\tau(\bar{x},\bar{y}) \\ = \prod_{\beta=1,2}\left(1+(-1)^{\beta-1}\bar{x}\right)^{\mu_\beta^\tau}\prod_{\beta=3,4}\left(1+(-1)^{\beta-1}\bar{y}\right)^{\mu_\beta^\tau} \tag{22}$$

Where β denotes the edge number and the exponents μ_β^τ can take the value 0 for free condition and the value 1 according to the conditions of held or straight for each displacement field $\tau \in \{u,v,w,\varphi_x,\varphi_y\}$. As can be seen in the right-hand side of Eq. (20), each displacement field $\tau \in \{u,v,w,\varphi_x,\varphi_y\}$ can be written as the product of a row vector $\boldsymbol{\mathcal{T}}_\tau^T$ containing the Legendre and boundary functions and a column vector $\boldsymbol{\mathcal{C}}_\tau$ containing the corresponding unknown collocation coefficients.

As mentioned before, the equilibrium equations are obtained based on the concept of the principle of minimum potential energy. Therefore, the elements in Eq. (12) should be written as described here. For this purpose, the vectors $\boldsymbol{u}$ and $\boldsymbol{\vartheta}$ can be rewritten in the compact matricial form

$$\boldsymbol{u} = \begin{bmatrix}\boldsymbol{\mathcal{T}}_u^T & 0 & 0\\ 0 & \boldsymbol{\mathcal{T}}_v^T & 0\\ 0 & 0 & \boldsymbol{\mathcal{T}}_w^T\end{bmatrix}\begin{Bmatrix}\boldsymbol{\mathcal{C}}_u\\ \boldsymbol{\mathcal{C}}_v\\ \boldsymbol{\mathcal{C}}_w\end{Bmatrix} = \begin{bmatrix}\boldsymbol{\Gamma}_u\\ \boldsymbol{\Gamma}_v\\ \boldsymbol{\Gamma}_w\end{bmatrix}\boldsymbol{U_u} = \boldsymbol{\Gamma_u U_u} \tag{23a}$$

$$\boldsymbol{\vartheta} = \begin{bmatrix}\boldsymbol{\mathcal{T}}_{\varphi_x}^T & 0\\ 0 & \boldsymbol{\mathcal{T}}_{\varphi_y}^T\\ 0 & 0\end{bmatrix}\begin{Bmatrix}\boldsymbol{\mathcal{C}}_{\varphi_x}\\ \boldsymbol{\mathcal{C}}_{\varphi_y}\end{Bmatrix} = \boldsymbol{\Gamma_\vartheta U_\vartheta} \tag{23b}$$

Accordingly, the strain vectors defined in Eq. (4) can also be rewritten as

$$\boldsymbol{\varepsilon}_p = \mathcal{B}_{p\boldsymbol{u}}\boldsymbol{U_u} \tag{24a}$$

$$\boldsymbol{\kappa} = \mathcal{B}_{p\boldsymbol{\vartheta}}\boldsymbol{U_\vartheta} \tag{24b}$$

$$\boldsymbol{\gamma} = \mathcal{B}_{n\boldsymbol{u}}\boldsymbol{U_u} + \mathcal{B}_{\boldsymbol{\vartheta}}\boldsymbol{U_\vartheta} \tag{24c}$$

$$\boldsymbol{\varepsilon}_{nl} = \frac{1}{2}\mathcal{B}_{nl\boldsymbol{u}}\boldsymbol{U_u} \tag{24d}$$

Where

$$\mathcal{B}_{p\boldsymbol{u}} = \boldsymbol{\mathcal{D}}_p\boldsymbol{\Gamma_u} \tag{25a}$$

$$\mathcal{B}_{p\boldsymbol{\vartheta}} = \boldsymbol{\mathcal{D}}_p\,\boldsymbol{\Gamma_\vartheta} \tag{25b}$$

$$\mathcal{B}_{\boldsymbol{\vartheta}} = \boldsymbol{\Gamma_\vartheta} \tag{25c}$$

$$\mathcal{B}_{n\boldsymbol{u}} = \boldsymbol{\mathcal{D}}_n\boldsymbol{\Gamma_u} \tag{25d}$$

$$\mathcal{B}_{nl\boldsymbol{u}} = \left(\boldsymbol{\mathcal{D}}_p \otimes \boldsymbol{\Gamma}_w\boldsymbol{U_u}\right)\boldsymbol{\mathcal{D}}_n\boldsymbol{\Gamma_u} \tag{25e}$$

And the total potential energy Π by using Eq. (24), can finally be written as

$$\begin{aligned}\Pi = \frac{1}{2}\iint_\Omega &\left(\boldsymbol{U_u^T}\left(\mathcal{B}_{p\boldsymbol{u}}^T\boldsymbol{A}_p\mathcal{B}_{p\boldsymbol{u}} + \mathcal{B}_{n\boldsymbol{u}}^T\boldsymbol{A}_n\mathcal{B}_{n\boldsymbol{u}}\right)\boldsymbol{U_u}\right.\\ &+\boldsymbol{U_u^T}\left(\mathcal{B}_{p\boldsymbol{u}}^T\boldsymbol{B}\mathcal{B}_{p\boldsymbol{\vartheta}} + \mathcal{B}_{n\boldsymbol{u}}^T\boldsymbol{A}_n\mathcal{B}_{\boldsymbol{\vartheta}}\right)\boldsymbol{U_\vartheta}\\ &+\boldsymbol{U_\vartheta^T}\left(\mathcal{B}_{p\boldsymbol{\vartheta}}^T\boldsymbol{B}\mathcal{B}_{p\boldsymbol{u}} + \mathcal{B}_{\boldsymbol{\vartheta}}^T\boldsymbol{A}_n\mathcal{B}_{n\boldsymbol{u}}\right)\boldsymbol{U_u}\\ &+\boldsymbol{U_\vartheta^T}\left(\mathcal{B}_{p\boldsymbol{\vartheta}}^T\boldsymbol{D}\mathcal{B}_{p\boldsymbol{\vartheta}} + \mathcal{B}_{\boldsymbol{\vartheta}}^T\boldsymbol{A}_n\mathcal{B}_{\boldsymbol{\vartheta}}\right)\boldsymbol{U_\vartheta}\\ &+\boldsymbol{U_u^T}\left(\frac{1}{2}\mathcal{B}_{p\boldsymbol{u}}^T\boldsymbol{A}_p\mathcal{B}_{nl\boldsymbol{u}} + \frac{1}{2}\mathcal{B}_{nl\boldsymbol{u}}^T\boldsymbol{A}_p\mathcal{B}_{p\boldsymbol{u}}\right)\boldsymbol{U_u}\\ &+\boldsymbol{U_u^T}\left(\frac{1}{2}\mathcal{B}_{nl\boldsymbol{u}}^T\boldsymbol{B}\mathcal{B}_{p\boldsymbol{\vartheta}}\right)\boldsymbol{U_\vartheta}\\ &+\boldsymbol{U_\vartheta^T}\left(\frac{1}{2}\mathcal{B}_{p\boldsymbol{\vartheta}}^T\boldsymbol{B}\mathcal{B}_{nl\boldsymbol{u}}\right)\boldsymbol{U_u}\\ &+\boldsymbol{U_u^T}\left(\frac{1}{4}\mathcal{B}_{nl\boldsymbol{u}}^T\boldsymbol{A}_p\mathcal{B}_{nl\boldsymbol{u}}\right)\boldsymbol{U_u}\\ &\left.-2\boldsymbol{U_u^T}\mathcal{B}_{p\boldsymbol{u}}^T\widetilde{\boldsymbol{\mathcal{F}}} + 2\boldsymbol{U_u^T}\mathcal{B}_{\boldsymbol{u}}^T\widetilde{\boldsymbol{\mathcal{P}}}\right)d\Omega\end{aligned} \tag{26}$$

Where $\mathcal{B}_u^T = \Gamma_u$. As noted before, the domain is discretized by a set of nodes in the current study, therefore the above continuous integrals should be replaced by summations which can be calculated over all nodes. For this purpose, Legendre-Gauss-Lobatto nodes that can be obtained by solving the following equations are established here

$$\begin{cases} \bar{x}_\zeta \ : \ P'_{m-1}(\bar{x}_\zeta) = 0 \\ \bar{y}_\eta \ : \ P'_{n-1}(\bar{y}_\eta) = 0 \end{cases} \tag{27}$$

Where the parameters m and n denote the number of nodes in *x* and *y* directions, respectively and $\bar{x}_\zeta$ and $\bar{y}_\eta$ are non-dimensional coordinates of ζ^{th} and η^{th} node in the *x* and *y* directions. Fig. 2 represents a scattered set of Legendre-Gauss-Lobatto nodes $(m \times n = 13 \times 13)$ in a typical domain Ω.

In order to achieve better accuracy and also to avoid the excessive number of nodes to reduce computational costs, an appropriate weight coefficient can be considered for each node. Calculation of the weight coefficients for nodes is performed by taking the idea from Gauss-Lobatto rules and therefore, the continuous integral of total potential energy (i.e., Eq. (26)) after eliminating the constant factors is then converted to the following relation

$$\begin{aligned} \Pi = \sum_{\zeta=1}^{m}\sum_{\eta=1}^{n} \varpi_\zeta \omega_\eta \Big\{ & \Big(\boldsymbol{U_u}^T \Big(\mathcal{B}_{p\boldsymbol{u}}^T \boldsymbol{A}_p^{\langle\zeta,\eta\rangle} \mathcal{B}_{p\boldsymbol{u}} \\ & + \mathcal{B}_{n\boldsymbol{u}}^T \boldsymbol{A}_n^{\langle\zeta,\eta\rangle} \mathcal{B}_{n\boldsymbol{u}} \Big) \boldsymbol{U_u} \\ & + \boldsymbol{U_u}^T \Big(\mathcal{B}_{p\boldsymbol{u}}^T \boldsymbol{B}^{\langle\zeta,\eta\rangle} \mathcal{B}_{p\boldsymbol{\vartheta}} + \mathcal{B}_{n\boldsymbol{u}}^T \boldsymbol{A}_n^{\langle\zeta,\eta\rangle} \mathcal{B}_{\boldsymbol{\vartheta}} \Big) \boldsymbol{U_\vartheta} \\ & + \boldsymbol{U_\vartheta}^T \Big(\mathcal{B}_{p\boldsymbol{\vartheta}}^T \boldsymbol{B}^{\langle\zeta,\eta\rangle} \mathcal{B}_{p\boldsymbol{u}} + \mathcal{B}_{\boldsymbol{\vartheta}}^T \boldsymbol{A}_n^{\langle\zeta,\eta\rangle} \mathcal{B}_{n\boldsymbol{u}} \Big) \boldsymbol{U_u} \\ & + \boldsymbol{U_\vartheta}^T \Big(\mathcal{B}_{p\boldsymbol{\vartheta}}^T \boldsymbol{D}^{\langle\zeta,\eta\rangle} \mathcal{B}_{p\boldsymbol{\vartheta}} + \mathcal{B}_{\boldsymbol{\vartheta}}^T \boldsymbol{A}_n^{\langle\zeta,\eta\rangle} \mathcal{B}_{\boldsymbol{\vartheta}} \Big) \boldsymbol{U_\vartheta} \\ & + \boldsymbol{U_u}^T \Big(\frac{1}{2} \mathcal{B}_{p\boldsymbol{u}}^T \boldsymbol{A}_p^{\langle\zeta,\eta\rangle} \mathcal{B}_{nl\boldsymbol{u}} + \frac{1}{2} \mathcal{B}_{nl\boldsymbol{u}}^T \boldsymbol{A}_p^{\langle\zeta,\eta\rangle} \mathcal{B}_{p\boldsymbol{u}} \Big) \boldsymbol{U_u} \\ & + \boldsymbol{U_u}^T \Big(\frac{1}{2} \mathcal{B}_{nl\boldsymbol{u}}^T \boldsymbol{B}^{\langle\zeta,\eta\rangle} \mathcal{B}_{p\boldsymbol{\vartheta}} \Big) \boldsymbol{U_\vartheta} \\ & + \boldsymbol{U_\vartheta}^T \Big(\frac{1}{2} \mathcal{B}_{p\boldsymbol{\vartheta}}^T \boldsymbol{B}^{\langle\zeta,\eta\rangle} \mathcal{B}_{nl\boldsymbol{u}} \Big) \boldsymbol{U_u} \\ & + \boldsymbol{U_u}^T \Big(\frac{1}{4} \mathcal{B}_{nl\boldsymbol{u}}^T \boldsymbol{A}_p^{\langle\zeta,\eta\rangle} \mathcal{B}_{nl\boldsymbol{u}} \Big) \boldsymbol{U_u} \\ & - 2\boldsymbol{U_u}^T \mathcal{B}_{p\boldsymbol{u}}^T \widetilde{\boldsymbol{\mathcal{F}}} + 2\boldsymbol{U_u}^T \mathcal{B}_{\boldsymbol{u}}^T \widetilde{\boldsymbol{\mathcal{P}}} \Big\} \Big|_{x=x_\zeta}^{y=y_\eta} \end{aligned} \tag{28}$$

Where $\langle\zeta,\eta\rangle$ indicates the ζ^{th} node in the *x*-direction and η^{th} node in the *y*-direction as represented in Fig. 2. The coefficients ϖ_ζ and ω_η are weight coefficients of nodes in the *x* and *y* directions, respectively and they can be computed by

$$\varpi_1 = \varpi_m = \frac{2}{m(m-1)}; \qquad \varpi_\zeta = \frac{2}{m(m-1)\big[P_{m-1}(\bar{x}_\zeta)\big]^2} \tag{29a}$$

$$\omega_1 = \omega_n = \frac{2}{n(n-1)}; \qquad \omega_\eta = \frac{2}{n(n-1)\big[P_{n-1}(\bar{y}_\eta)\big]^2} \tag{29b}$$

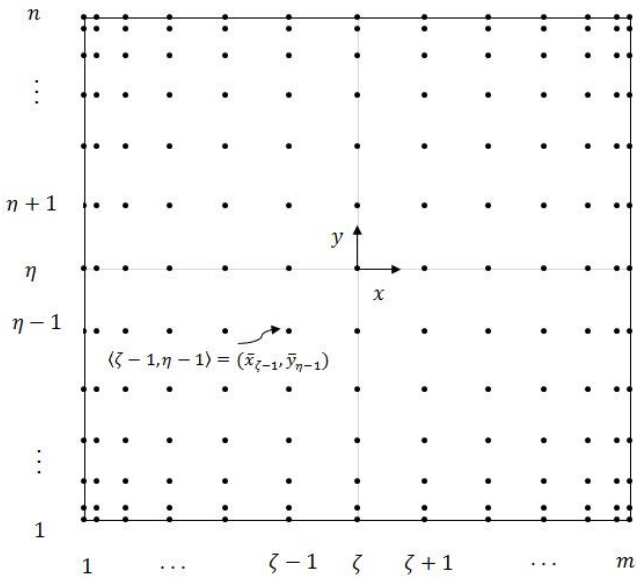

Fig. 2 Discretized plate model

To obtain the equilibrium equations of the problem using the principle of minimum potential energy, the discretized form of the total potential energy Eq. (28) should be minimized with respect to the unknown primary variables $\boldsymbol{U_u}$ and $\boldsymbol{U_\vartheta}$ (i.e., $\partial\Pi/\partial\boldsymbol{U_u} = 0$ and $\partial\Pi/\partial\boldsymbol{U_\vartheta} = 0$). Therefore, the final set of equilibrium equations can be written as

$$\begin{aligned} & \left\{ \sum_{\zeta=1}^{m}\sum_{\eta=1}^{n} \varpi_\zeta \omega_\eta \Big(\mathcal{B}_{p\boldsymbol{u}}^T \boldsymbol{A}_p^{\langle\zeta,\eta\rangle} \mathcal{B}_{p\boldsymbol{u}} + \mathcal{B}_{n\boldsymbol{u}}^T \boldsymbol{A}_n^{\langle\zeta,\eta\rangle} \mathcal{B}_{n\boldsymbol{u}} \Big) \Big|_{x=x_\zeta}^{y=y_\eta} \right\} \boldsymbol{U_u} \\ & + \left\{ \sum_{\zeta=1}^{m}\sum_{\eta=1}^{n} \varpi_\zeta \omega_\eta \Big(\mathcal{B}_{p\boldsymbol{u}}^T \boldsymbol{B}^{\langle\zeta,\eta\rangle} \mathcal{B}_{p\boldsymbol{\vartheta}} + \mathcal{B}_{n\boldsymbol{u}}^T \boldsymbol{A}_n^{\langle\zeta,\eta\rangle} \mathcal{B}_{\boldsymbol{\vartheta}} \Big) \Big|_{x=x_\zeta}^{y=y_\eta} \right\} \boldsymbol{U_\vartheta} \\ & + \left\{ \sum_{\zeta=1}^{m}\sum_{\eta=1}^{n} \varpi_\zeta \omega_\eta \Big(\frac{3}{4} \mathcal{B}_{nl\boldsymbol{u}}^T \boldsymbol{A}_p^{\langle\zeta,\eta\rangle} \mathcal{B}_{p\boldsymbol{u}} \right. \\ & \qquad \left. + \frac{3}{4} \mathcal{B}_{p\boldsymbol{u}}^T \boldsymbol{A}_p^{\langle\zeta,\eta\rangle} \mathcal{B}_{nl\boldsymbol{u}} \Big) \Big|_{x=x_\zeta}^{y=y_\eta} \right\} \boldsymbol{U_u} \\ & + \left\{ \sum_{\zeta=1}^{m}\sum_{\eta=1}^{n} \varpi_\zeta \omega_\eta \Big(\mathcal{B}_{nl\boldsymbol{u}}^T \boldsymbol{B}^{\langle\zeta,\eta\rangle} \mathcal{B}_{p\boldsymbol{\vartheta}} \Big) \Big|_{x=x_\zeta}^{y=y_\eta} \right\} \boldsymbol{U_\vartheta} \\ & + \left\{ \sum_{\zeta=1}^{m}\sum_{\eta=1}^{n} \varpi_\zeta \omega_\eta \Big(\frac{1}{2} \mathcal{B}_{nl\boldsymbol{u}}^T \boldsymbol{A}_p^{\langle\zeta,\eta\rangle} \mathcal{B}_{nl\boldsymbol{u}} \Big) \Big|_{x=x_\zeta}^{y=y_\eta} \right\} \boldsymbol{U_u} \\ & = \left\{ \sum_{\zeta=1}^{m}\sum_{\eta=1}^{n} \varpi_\zeta \omega_\eta \{ \mathcal{B}_{p\boldsymbol{u}}^T \} \Big|_{x=x_\zeta}^{y=y_\eta} \right\} \widetilde{\boldsymbol{\mathcal{F}}} \\ & \qquad - \left\{ \sum_{\zeta=1}^{m}\sum_{\eta=1}^{n} \varpi_\zeta \omega_\eta \{ \mathcal{B}_{\boldsymbol{u}}^T \} \Big|_{x=x_\zeta}^{y=y_\eta} \right\} \widetilde{\boldsymbol{\mathcal{P}}} \end{aligned} \tag{30}$$

$$\left\{\sum_{\zeta=1}^{m}\sum_{\eta=1}^{n}\varpi_\zeta\omega_\eta\left(\mathcal{B}_{p\vartheta}^{T}\boldsymbol{B}^{\langle\zeta,\eta\rangle}\mathcal{B}_{p\boldsymbol{u}}+\mathcal{B}_{\vartheta}^{T}\boldsymbol{A}_{n}^{\langle\zeta,\eta\rangle}\mathcal{B}_{n\boldsymbol{u}}\right)\Big|_{x=x_\zeta}^{y=y_\eta}\right\}\boldsymbol{U}_{\boldsymbol{u}}$$
$$+\left\{\sum_{\zeta=1}^{m}\sum_{\eta=1}^{n}\varpi_\zeta\omega_\eta\left(\mathcal{B}_{p\vartheta}^{T}\boldsymbol{D}^{\langle\zeta,\eta\rangle}\mathcal{B}_{p\vartheta}+\mathcal{B}_{\vartheta}^{T}\boldsymbol{A}_{n}^{\langle\zeta,\eta\rangle}\mathcal{B}_{\vartheta}\right)\Big|_{x=x_\zeta}^{y=y_\eta}\right\}\boldsymbol{U}_{\vartheta} \quad (31)$$
$$+\left\{\sum_{\zeta=1}^{m}\sum_{\eta=1}^{n}\varpi_\zeta\omega_\eta\left(\frac{1}{2}\mathcal{B}_{p\vartheta}^{T}\boldsymbol{B}^{\langle\zeta,\eta\rangle}\mathcal{B}_{nl\boldsymbol{u}}\right)\Big|_{x=x_\zeta}^{y=y_\eta}\right\}\boldsymbol{U}_{\vartheta}=\boldsymbol{0}$$

The above nonlinear sets of equations are solved iteratively to satisfy the preceding criteria mentioned in section 3.

5. Damage models

In this section, the methodology of progressive damage analysis including the failure criteria, material degradation model and ply geometric degradation models is described in details.

5.1 Failure criteria

To determine the failure load and the corresponding failure mode, Hashin failure criterion is used in the present study (Hashin and Rotem 1973). This criterion includes four different damage functions which correspond to the different modes of failure namely fiber tension, fiber compression, matrix tension, and matrix compression as given in Table 1.

Table 1 Four different damage functions in Hashin criterion

Failure mode	Mathematical model	Damage function
Fiber failure in tension	$\sigma_1 \geq 0$	$\mathbb{f}_f^T = \left(\frac{\sigma_1}{X_T}\right)^2$
Fiber failure in compression	$\sigma_1 < 0$	$\mathbb{f}_f^C = \left(\frac{\sigma_1}{X_C}\right)^2$
Matrix failure in tension	$\sigma_2 \geq 0$	$\mathbb{f}_m^T = \left(\frac{\sigma_2}{Y_T}\right)^2 + \left(\frac{\tau_{12}}{S_{12}}\right)^2$
Matrix failure in compression	$\sigma_2 < 0$	$\mathbb{f}_m^C = \left(\frac{\sigma_2}{Y_C}\right)^2 + \left(\frac{\tau_{12}}{S_{12}}\right)^2$

In this table, X_T and X_C denote tensile and compressive strengths of fiber and Y_T and Y_C are tensile and compressive strengths of the matrix, respectively. Failure happens when any of these modes reaches unity.

5.2 Material degradation model

As it is known, when damage occurs in a composite structure, the effective material properties are reduced. This reduction can be modeled in this study by the following matrix.

$$\boldsymbol{Q}_p = \frac{1}{\Delta}\begin{bmatrix} d_f E_1 & d_f d_m \nu_{12} E_2 & 0 \\ d_f d_m \nu_{21} E_1 & d_m E_2 & 0 \\ 0 & 0 & d_f d_m \Delta G_{12} \end{bmatrix} \quad (32)$$
$$\Delta = 1 - d_f d_m \nu_{21}\nu_{12}$$

Where E_1, E_2, G_{12}, ν_{12} and ν_{21} are undamaged material properties. The parameters d_f and d_m are the damage factors in fiber and matrix directions, respectively. According to the degradation model presented by Hayman *et al*. (2011) and Yang *et al*. (2013), the transverse shear stiffness matrix Q_n is not degraded during the damage analysis.

In the current progressive damage model, the reduction of material properties is considered to happen instantaneously. When failure is detected in the specific zone (complete, region or node), its properties are instantaneously reduced to %1 of their initial and undamaged values (i.e., d_f or $d_m = 0.01$).

5.3 Ply geometric degradation models

In this study, two or three geometric degradation models depend on the type of numerical method (Rayleigh-Ritz or collocation) are assumed to estimate the degradation zone around the failure location which are named complete, region and node degradation models. When the failure occurs in a location, the material properties of its zone should be reduced as:

(1) Complete Degradation Model (CDM) in which, the material properties of the entire ply are reduced.

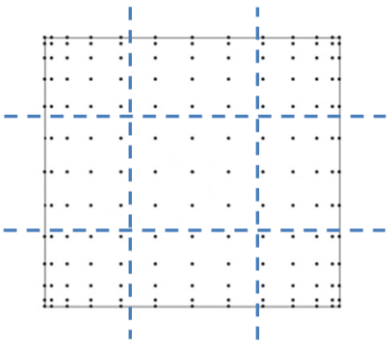

(a)

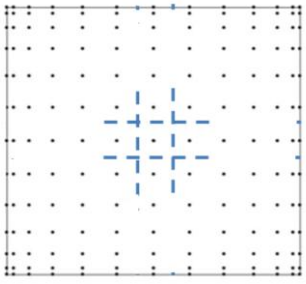

(b)

Fig. 3 Ply geometric degradation models around the location failure: (a) Region degradation model (RDM); (b) Node degradation model (NDM)

(2) Region Degradation Model (RDM) in which a plate is divided into 9 regions and material properties of the region where failure has occurred are reduced. (as illustrated in Fig. 3(a)).
(3) Node Degradation Model (NDM) in which, the material properties of the area around the failed node are reduced. (as illustrated in Fig. 3(b))

Both CDM and RDM models can be used in the Rayleigh-Ritz method but the third model (i.e., NDM) is not applicable due to the lack of nodes in mathematical modeling of the plate in this method.

6. Numerical results and discussion

6.1 Geometry and material properties

The square laminated plates with dimension $a = 500$ are investigated in this section. Their layups are assumed to be $[0/45/90/\text{-}45]_{X,s}$. The thickness of each layer is 1 mm and X gets the values "$X = 2, 3, 4, 6$", The material properties for each lamina are assumed as

$$E_1 = 49627 \text{ MPa}, E_2 = 15430 \text{ MPa}, \vartheta_{12} = 0.272,$$
$$G_{12} = G_{23} = G_{13} = 4800 \text{ MPa},$$
$$X_t = 968 \text{ MPa}, \quad X_c = 915 \text{ Mpa}, \quad Y_t = 24 \text{ Mpa},$$
$$Y_c = 118 \text{ MPa}, \quad S_{12} = 65 \text{ MPa}$$

It is noted that to apply the ply region degradation model, it is necessary to define the size of the regions shown in Fig. 3 whose values can be found in Table 2.

Table 2 Assumed sizes for regions in NDM model

Region	Dimensions ($mm \times mm$)
1, 3, 7 and 9	160×160
2 and 8	180×160
4 and 6	160×180
5	180×180

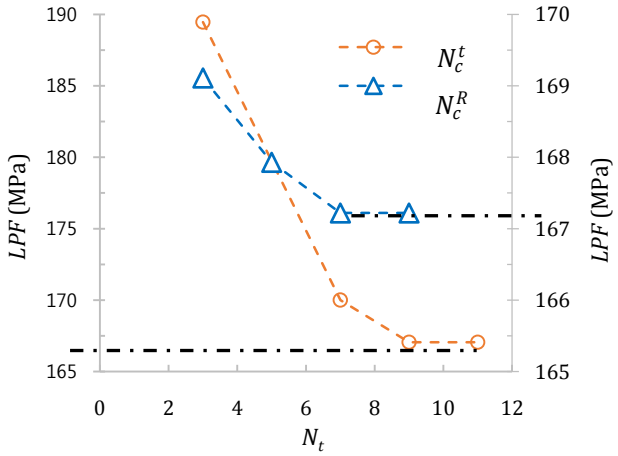

Fig. 4 Convergence study of ultimate in-plane load with regard to the number of terms for 24 mm laminate under $Q = 2$

In order to show the results, a pressure load factor is defined as $Q = nP_0a^3/8D_{22}$. Parameter n is the number of layers in the laminates and P_0 is the magnitude of the applied pressure load.

6.2 Convergence study

In order to do the convergence analysis and to find the sufficient number of terms in the displacement fields in both methods (N_t^R and N_t^C), ultimate in-plane load or last ply failure (LPF) stress of square laminated plate under in-plane load with boundary condition type A and with layup $[0/45/90/-45]_{3s}$ have been calculated for different number of terms. To obtain the results, a uniform pressure load factor $Q = 2$ is also assumed to be applied on the plate. Fig. 5 represents the convergence study of ultimate in-plane load with regard to the number of terms in both Rayleigh-Ritz and collocation method.

According to Fig. 4, it can be observed that the converged results are obtained by considering 9×9 terms (i.e., $N_t^R = N_t^C = 9$) in each displacement field for both Rayleigh-Ritz and collocation methods. Therefore, the total number of unknown coefficients is 407 for both methods.

Also, similar analyzes have been conducted in collocation method with regards to the number of nodes for all three geometric degradation models and it was concluded that the total number of 121 nodes ($m \times n = 11 \times 11$) are sufficient to obtain converged results.

6.3 Verification of the formulation

In order to verify the proposed formulations, finite element model without taking account of the damage is also analyzed. Laminate with 24 mm thickness (i.e., $X = 3$) and for two different values of lateral pressure load factors is studied here. The magnitude of load factors is selected to be $Q = 1$ and $Q = 3$. Boundary conditions of the laminates are also considered to be type A. The finite element analysis is carried out using static general solver of ABAQUS software package. The plates are meshed using four-node quadrilateral shell element with reduced integration (S4R). Through the convergence study it was found that a mesh of 40×40 S4R elements could give accurate results. Also in this software, the interaction module has been used to create straight boundary conditions on edges.

As it can be seen from the Figs. 5-6, there is an excellent agreement between the results obtained by all three methods.

6.4 Results for boundary condition type A

Both Rayleigh-Ritz and collocation methods have been used here to analyze the laminates with boundary condition type A. In analyzing the laminates using Rayleigh-Ritz method, both complete and region degradation models (CDM and RDM) are considered while in collocation method, only complete degradation model is taken into account. All results obtained here are compared with each other and presented in appropriate tables and figures. To

Table 3 The results for complete ply degradation model using Rayleigh-Ritz method (type A)

X (Number of layers)	Pressure load factor (Q)	FPF stress (MPa)	Ply No. (coordinates of failure)	LPF stress (MPa)	Ply No. (coordinates of failure)	No. of plies with failed matrix	No. of plies with failed fiber
2(16)	0	92.89	16(0,0)	134.70	2(-250,250)	16	2
	1	68.75	16(0,0)	131.84	2(-250,250)	16	2
	2	47.20	16(0,0)	129.14	2(-250,250)	16	2
	3	27.61	16(0,0)	126.56	2(-250,250)	16	2
	4.54	0	16(0,0)	121.82	2(-250,250)	16	2
3(24)	0	205.23	22(0,0)	205.23	22(0,0)	1	0
	1	143.62	24(0,0)	172.58	23(-250,-250)	24	1
	2	93.58	24(0,0)	167.22	23(-250,-250)	24	1
	3	50.25	24(0,0)	162.25	2(-250,250)	24	2
	4.34	0	24(0,0)	155.25	2(-250,250)	24	2
4(32)	0	209.14	3(-250,-250)	281.30	1(0,0)	25	0
	1	190.39	3(0,0)	232.60	1(0,0)	28	1
	2	144.98	32(0,0)	218.55	1(0,0)	28	1
	3	74.85	32(0,0)	205.80	1(0,0)	29	1
	4.27	0	32(0,0)	195.03	1(0,0)	29	1

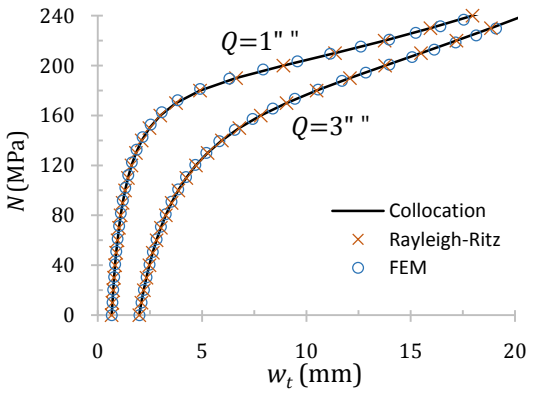

Fig. 5 Response of load vs central out-of-plane displacement for 24 mm laminates (boundary conditions type A)

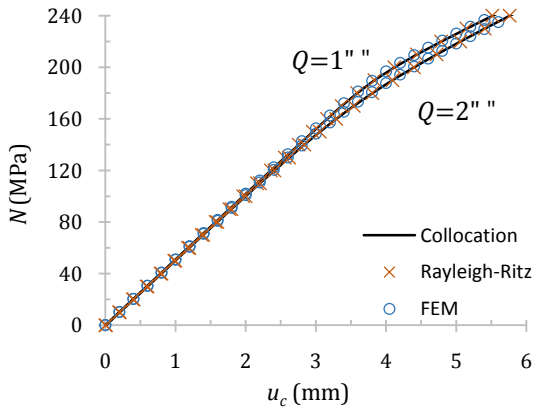

Fig. 6 Response of load vs end shortening displacement for 24 mm laminates (boundary conditions type A)

this end, the results of Rayleigh-Ritz method considering the CDM model are tabulated in Table 3.

Similar results obtained by collocation method considering the CDM model are tabulated in Table 4.

The presented results have been computed for composite plates with 16, 24 and 32 mm thicknesses and for 5 different values of lateral pressure load factors. The magnitude of load factors is selected to be $Q = 0, 1, 2, 3, Q_s$. The parameter Q_s in which the first ply failure (FPF) occurs in zero longitudinal stress, is called a specific load factor. In these tables, the first ply failure load (i.e., The longitudinal applied load in which the first ply is failed) and location of the failure in terms of ply number and coordinates of the failure point have been included. The ultimate strength or last ply failure (LPF) stress (i.e., The longitudinal applied load after which no lamina can withstand load), the failure location (i.e., ply number and coordinates of failure point) and the number of layers whose matrix or fiber fails, are also included in these tables.

According to Tables 3 and 4, it is seen that by increasing the number of plies first ply failure stress and ultimate load are increased. It is also observed that the FPF almost occurs in the center of the last layer and in most cases, the ultimate load coincides with the fiber failure. Based on the observations, it can be stated that for 0^o and 90^o plies failure often occurs first in the center of the plate, while it happens at the corners for $\pm 45^o$ plies.

Furthermore, to describe the progressive damage behavior, the variation of load in terms of end-shortening displacement and also the variation of load versus out-of-plane-displacement for some selected results given in these tables, are depicted in the following figures. Solid and hollow circles in these figures, indicate the first ply failure and last ply failure stresses of the laminates, respectively. The important consequence of the results presented in both

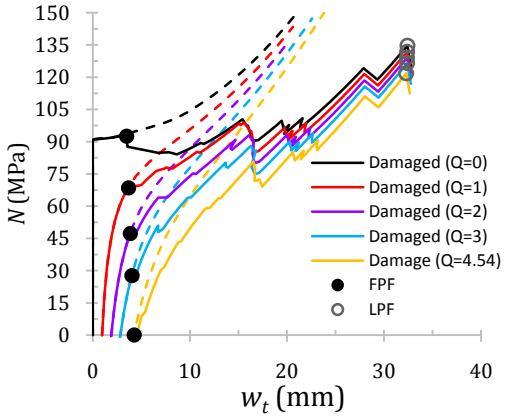

Fig. 7 Response of load vs central out-of-plane displacement for 16 mm laminate using Rayleigh-Ritz method and CDM model (type A)

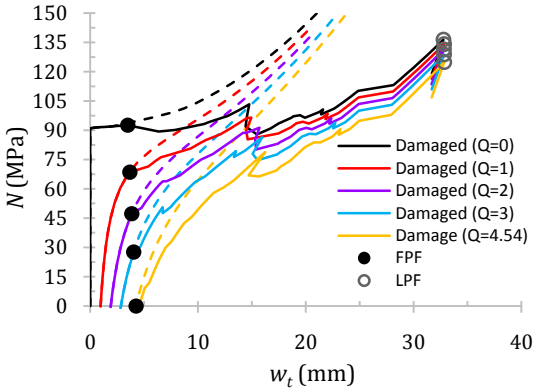

Fig. 9 Response of load vs central out-of-plane displacement for 16 mm laminate using Collocation method and CDM model (type A)

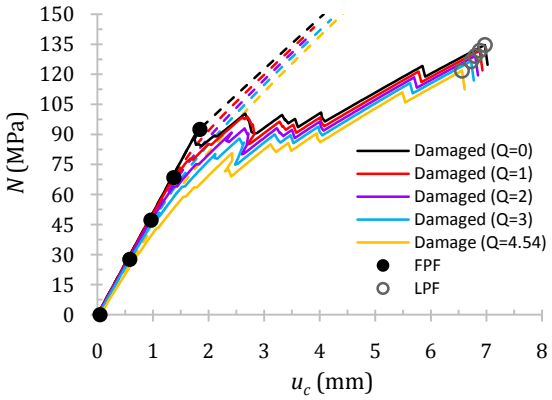

Fig. 8 Response of load vs end shortening for 16 mm laminate using Rayleigh-Ritz method and CDM model (type A)

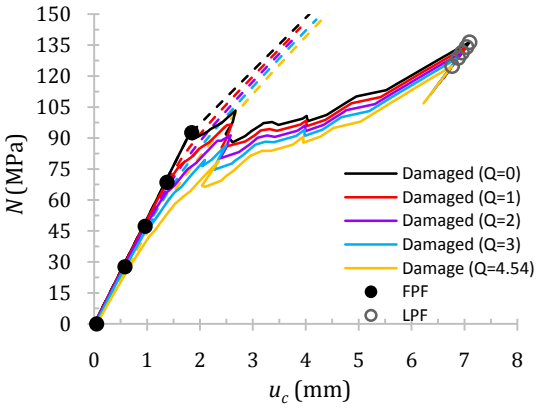

Fig. 10 Response of load vs end shortening for 16 mm laminate using Collocation method and CDM model (type A)

Table 4 The results for complete ply degradation model using Collocation method (type A)

X (Number of layers)	Pressure load factor (Q)	FPF stress (MPa)	Ply No. (coordinates of failure)	LPF stress (MPa)	Ply No. (coordinates of failure)	No. of plies with failed matrix	No. of plies with failed fiber
2(16)	0	92.53	16(0,0)	136.36	2(250,-210)	16	2
	1	68.50	16(0,0)	134.05	2(250, -210)	16	2
	2	47.25	16(0,0)	131.34	2(250, -210)	16	2
	3	27.62	16(0,0)	128.77	2(250, -210)	16	2
	4.54	0	16(0,0)	124.84	2(250, -210)	16	2
3(24)	0	205.49	22(0,0)	205.49	22(0,0)	1	0
	1	143.00	24(0,0)	168.57	1(10, 100)	24	2
	2	92.75	24(0,0)	167.05	1(10, 110)	24	2
	3	50.12	24(0,0)	164.69	1(10, 110)	24	2
	4.34	0	24(0,0)	158.74	2(250,-220)	24	2
4(32)	0	209.00	3(-250,-250)	279.93	1(0,0)	25	0
	1	190.25	3(0,0)	232.12	1(0,0)	28	1
	2	144.25	32(0,0)	215.34	1(0,0)	29	1
	3	75.00	32(0,0)	203.47	5(-250,-250)	30	0
	4.27	0	32(0,0)	192.05	1(0,0)	30	1

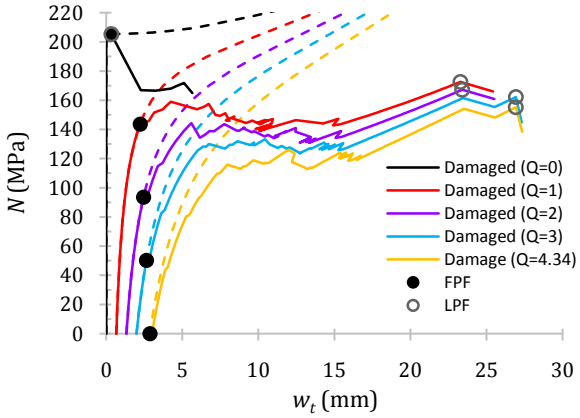

Fig. 11 Response of load vs central out-of-plane displacement for 24 mm laminate using Rayleigh-Ritz method and CDM model (type A)

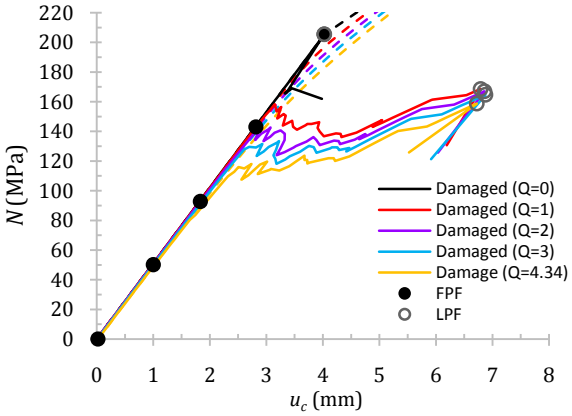

Fig. 14 Response of load vs end shortening for 24 mm laminate using Collocation method and CDM model (type A)

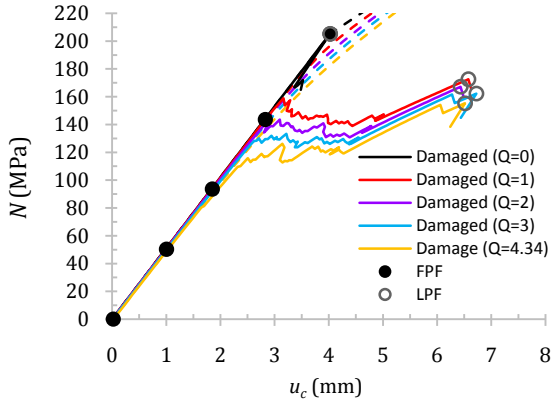

Fig. 12 Response of load vs end shortening for 24 mm laminate using Rayleigh-Ritz method and CDM model (type A)

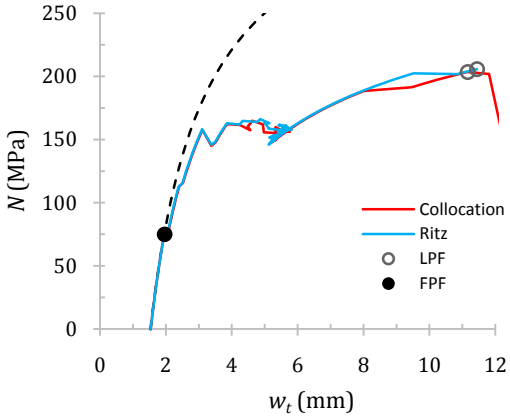

Fig. 15 Response of Load vs central out-of-plane displacement for 32 mm laminate with $Q = 3$ and CDM model (Rayleigh-Ritz and Collocation methods)

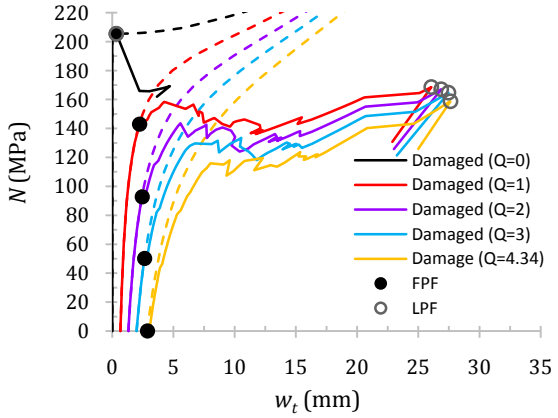

Fig. 13 Response of load vs central out-of-plane displacement for 24 mm laminate using Collocation method and CDM model (type A)

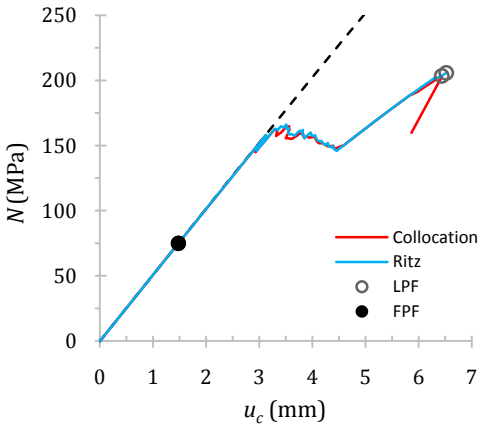

Fig. 16 Response of Load vs end shortening for 32 mm laminate with $Q = 3$ and CDM model (Rayleigh-Ritz and Collocation methods)

tables and figures is that by increasing the load factor Q the last ply and first ply failure stresses are decreased but the last ply failure stresses are reduced much lower than first ply failure loads.

In these figures, nonlinear behaviors of the plates with and without taking account of damage have been shown. Undamaged results have been displayed by dashed lines and the damaged results have been displayed by solid lines.

In order to better comparison between two methods, the

Table 5 The results for region ply degradation model using Rayleigh-Ritz method (type A)

X (Number of layers)	Pressure load factor (Q)	FPF stress (MPa)	Ply No. (coordinates of failure)	LPF stress (MPa)	Ply No. (coordinates of failure)	No. of plies with failed matrix	No. of plies with failed fiber
2(16)	1	68.75	16(0,0)	145.47	133	4	131.84
	2	47.20	16(0,0)	143.46	133	4	129.14
	3	27.61	16(0,0)	140.40	130	4	126.56
	4.54	0	16(0,0)	136.64	130	4	121.82
3(24)	1	143.62	24(0,0)	169.51	208	1	172.58
	2	93.58	24(0,0)	167.18	208	1	167.22
	3	50.25	24(0,0)	164.38	208	3	162.25
	4.34	0	24(0,0)	163.06	204	3	155.25
4(32)	1	190.39	3(0,0)	232.63	252	1	232.60
	2	144.98	32(0,0)	218.61	252	1	218.55
	3	74.85	32(0,0)	204.43	253	1	205.80
	4.27	0	32(0,0)	191.04	252	1	195.03

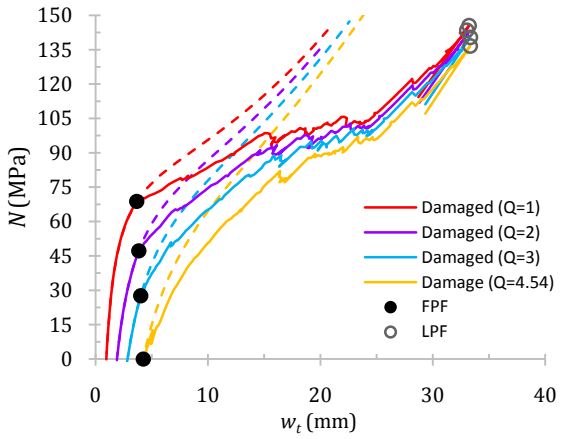

Fig. 17 Response of load vs central out-of-plane displacement for 16 mm laminate using Rayleigh-Ritz method and RDM model (type A)

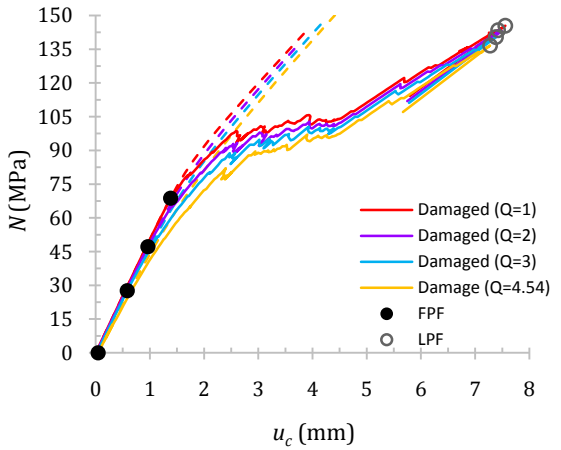

Fig. 18 Response of load vs end shortening for 16 mm laminate using Rayleigh-Ritz method and RDM model (type A)

results obtained by both formulations for laminate with 32 mm thickness and for pressure load factor 3 are represented in Figs. 15-16.

In addition to previous results, the results for region degradation model (RDM) using the Rayleigh-Ritz method are also presented and investigated here. Table 5 shows the results for composite plates having boundary conditions type A. Similar to before, first ply failure stresses and locations have been achieved. Also in the table, last ply failure stresses and the number of matrix and fiber failed regions are included for each laminate thickness and load factor.

As respected, it can be observed that there is no difference between the first ply failure loads obtained by both CDM and RDM models. However, in most cases, the CDM model gives generally slightly lower ultimate loads than the RDM model. In Figs. 18 and 19, the applied load is plotted against the central out-of-plane displacement and end shortening displacement respectively, for plates having the total thickness of 16 mm.

The behaviors of the load against central out-of-plane displacement and load against end-shortening displacement for plates with $h = 24$ mm and values of load factor $Q = 3$ are depicted in Figs. 19-20. In these figures, in addition to the results obtained by RDM model, and results of CDM using the Rayleigh-Ritz method are also represented.

At the end of this section, in order to better understanding the behavioral differences of the laminates with different thicknesses in progressive damage process, the results with pressure load factor $Q = 2$ are depicted in Figs. 21-22.

As it can be seen by increasing the thickness of the laminates, first ply failure and last ply failure occur in the higher amount of load. This is while the amounts of end shortening displacements corresponding to the first ply failure loads decrease.

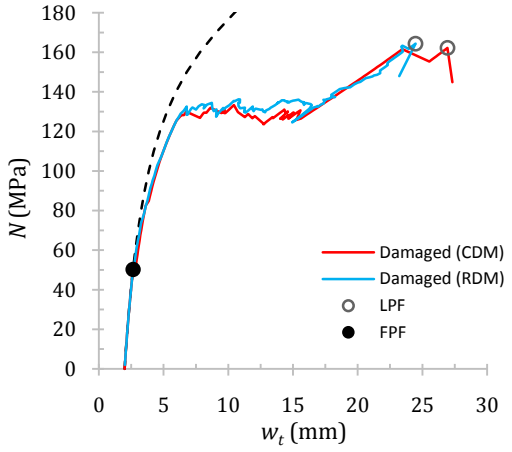

Fig. 19 Response of Load vs central out-of-plane displacement for 24 mm laminate with $Q = 3$ using Rayleigh-Ritz method by CDM and RDM (type A)

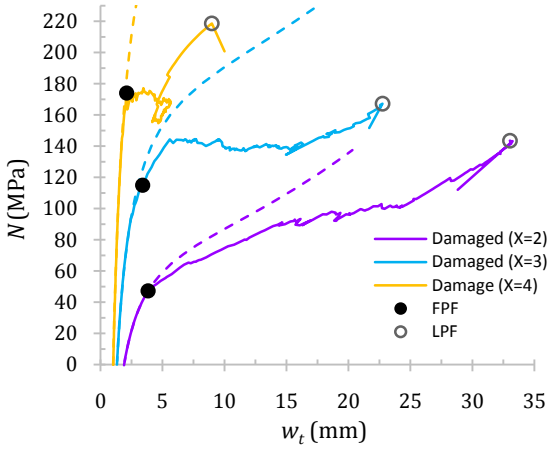

Fig. 21 Response of Load vs central out-of-plane displacement for 16 mm, 24 mm and 32 mm laminates with $Q = 2$ using Rayleigh-Ritz and RDM (type A)

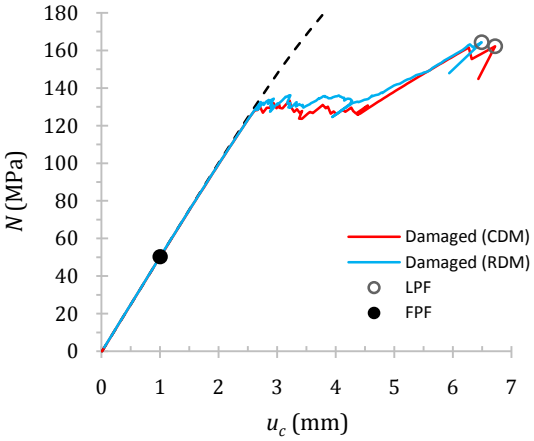

Fig. 20 Response of Load vs end shortening for 24 mm laminate with $Q = 3$ using Rayleigh-Ritz method by CDM and RDM (type A)

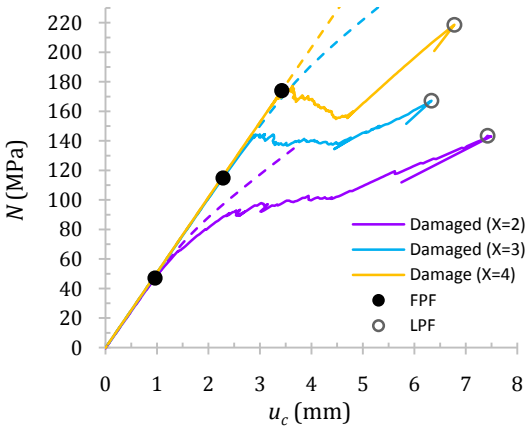

Fig. 22 Response of Load vs end shortening for 16 mm, 24 mm and 32 mm laminates with $Q = 2$ using Rayleigh-Ritz and RDM (type A)

6.5 Results for boundary condition type B

Another category of results for the second boundary conditions (type B) is presented in this section. In the Rayleigh-Ritz method only the results associated with the CDM model are computed and in the collocation method, the results associated with all ply geometric degradation models (i.e., CDM, RDM, and NDM) are calculated and presented. The results in this section have been calculated with enough number of terms. These results are tabulated in

Table 6The results for complete ply degradation model using Rayleigh-Ritz method (type B)

X (Number of layers)	Pressure load factor (Q)	FPF stress (MPa)	Ply No. (coordinates of failure)	LPF stress (MPa)	Ply No. (coordinates of failure)	No. of plies with failed matrix	No. of plies with failed fiber
3(24)	1	201.00	3(0,0)	255.70	1(0,0)	24	1
	2	98.05	1(0,0)	247.46	1(0,0)	24	1
4(32)	1	202.41	3(0,0)	297.23	1(0,0)	30	1
	2	133..10	1(0,0)	288.29	1(0,0)	32	1
6(48)	1	203.20	3(0,0)	302.65	1(0,0)	38	1
	2	181.23	3(0,0)	297.01	1(0,0)	45	1

Table 7 The results for complete ply degradation model using Collocation method (type B)

X (Number of layers)	Pressure load factor (Q)	FPF stress (MPa)	Ply No. (coordinates of failure)	LPF stress (MPa)	Ply No. (coordinates of failure)	No. of plies with failed matrix	No. of plies with failed fiber
3(24)	1	200.97	3(0,0)	253.47	1(0,0)	24	1
	2	97.87	1(-10,0)	245.28	1(0,0)	24	1
4(32)	1	202.19	3(0,0)	296.94	1(0,0)	31	1
	2	132.01	1(10,250)	288.31	1(0,0)	32	1
6(48)	1	203.34	3(0,0)	302.94	1(0,0)	39	1
	2	180.00	1(0,-250)	296.66	1(0,0)	45	1

Table 8 The results for region ply degradation model using Collocation method (type B)

Number of layers	Pressure load factor (Q)	FPF stress (MPa)	Ply No. (coordinates of failure)	LPF stress (MPa)	Number of regions with failed matrix	Number of regions with failed fiber	LPF stress (MPa) CMD
3(24)	1	200.97	3(0,0)	257.36	207	1	253.47
	2	97.87	1(-10,0)	247.43	207	1	245.28
4(32)	1	202.19	3(0,0)	297.91	253	1	296.94
	2	132.01	1(10,250)	288.91	268	0	288.31
6(48)	1	203.34	3(0,0)	303.23	346	1	302.94
	2	180.00	1(0,-250)	297.61	380	1	296.66

Tables 6 to 9. Similar to the previous section, first and last ply failure loads are reported in these tables. Moreover, the number of failed zones (ply, region or node) in each fiber or matrix mode is also given.

It can be observed that the laminate under a small pressure load factor fails first in the third layer, while at larger value of pressure load factor laminates fail often in the first layer. In the case of LPF, all plates with all pressure load factors fail in the center of the first layer and in fiber mode.

In Figs. 23-24, the applied load is plotted against the central out-of-plane displacement and end shortening displacement respectively, for plates having the total thickness of 24 mm and $Q = 2$. In order to better comparison, the results for boundary conditions type A are also represented in these figures. It is noted that the results presented in these figures are computed by the Rayleigh-Ritz method.

As it is apparent in Figs. 23-24, ultimate load of the laminates with boundary condition type A are much smaller than those with boundary condition type B. This also occurs at smaller values of end shortening displacement. In Collocation method, the results associated with region and node degradation models (RDM and NDM) have been also obtained. Tables 8 and 9 show these results for composite

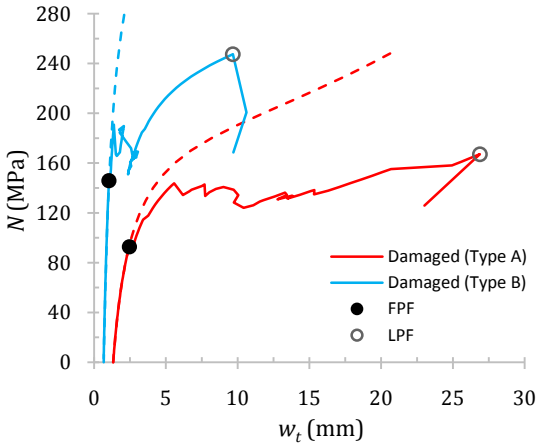

Fig. 23 Response of load vs central out-of-plane displacement for 24 mm laminate with $Q = 2$ using Rayleigh-Ritz method and CDM model (types A and B)

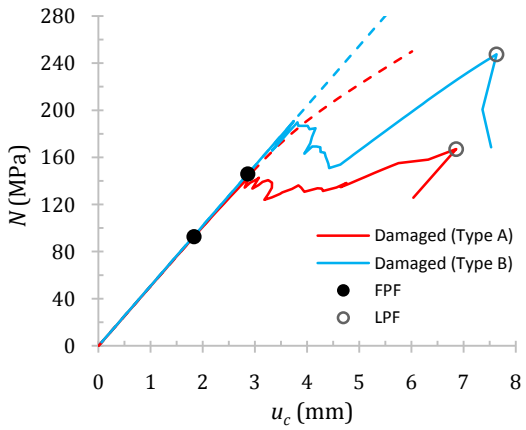

Fig. 24 Response of load vs end shortening for 24 mm laminate with $Q = 2$ using Rayleigh-Ritz method and CDM model (types A and B)

Table 9 The results for node ply degradation model using Collocation method (type B)

Number of layers	Pressure load factor (Q)	FPF stress (MPa)	Ply No. (coordinates of failure)	LPF stress (MPa)	Number of regions with failed matrix	Number of regions with failed fiber	LPF stress (MPa) CMD
3(24)	1	200.97	3(0,0)	264.82	2435	1	253.47
	2	97.87	1(-10,0)	252.02	2463	1	245.28
4(32)	1	202.19	3(0,0)	299.09	3040	1	296.94
	2	132.01	1(10,250)	290.49	3137	1	288.31

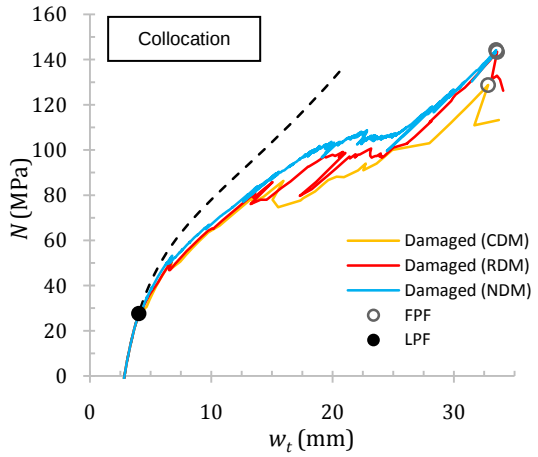

Fig. 25 Response of load vs central out-of-plane displacement, compression between degradation model for 24 mm laminate with $Q = 3$ using Collocation method (type A)

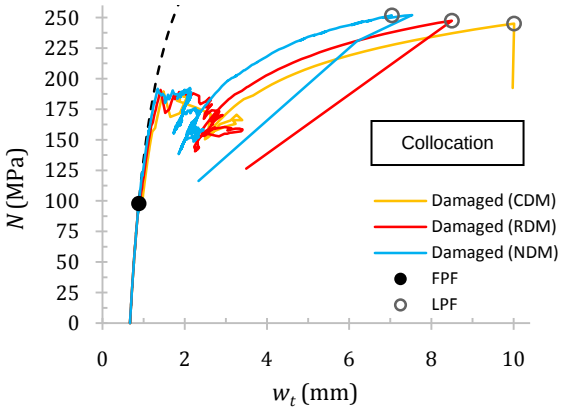

Fig. 27 Response of load vs central out-of-plane displacement, compression between degradation model for 24 mm laminate with $Q = 2$ using Collocation method (type B)

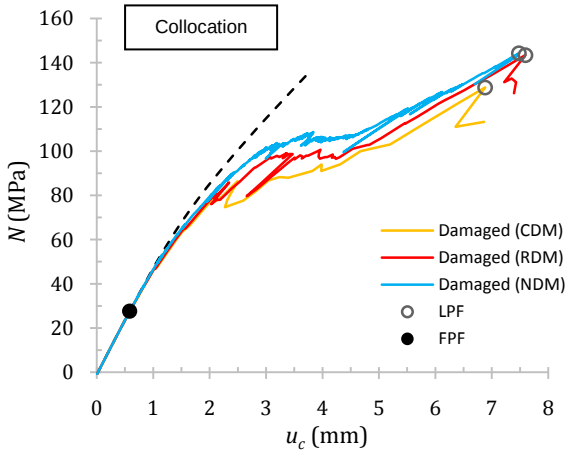

Fig. 26 Response of load vs end shortening, compression between degradation model for 24 mm laminate with $Q = 3$ using Collocation method (type A)

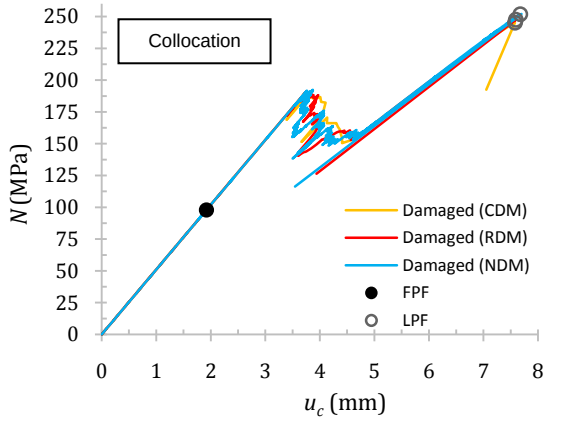

Fig. 28 Response of load vs end shortening, compression between degradation model for 24 mm laminate with $Q = 2$ using Collocation method (type B)

plates having boundary conditions type B. As before, first ply failure stresses and locations have been achieved. In these tables, last ply failure stresses and the number of matrix and fiber failed regions and nodes are reported for some load factor values.

The behaviors of load against central out-of-plane displacement and load against end-shortening displacement for plates having the total thickness of 24 mm and different values of load factor and boundary condition are depicted in Figs. 25-28. In these figures, in addition to the results obtained by NDM, the results taken from two other models, are also represented.

As it can be observed, there is no difference between the values of first ply failure loads calculated by three degradation models as expected however, the complete model gives generally slightly lower values of the ultimate load than the two others.

With the comparison between three degradation models,

it is seen that the node degradation model gives upper last ply failure load and this can be due to the effects of dividing the plate (or ply) into smaller areas. Therefore, if one wants to obtain better and more accurate results, NDM should be used in which more computation time is also needed but in the early stages of structural design; the results taken from RDM can be accepted with lightly lower accuracy.

7. Conclusions

Two methods were proposed in this study to investigate the ultimate strength of composite plates under combined in-plane and lateral pressure loads. Laminates with two different types of boundary conditions were studied. The concept of the first order shear deformation theory was established to drive the equilibrium equations. The onset of damage was predicted by Hashin's failure criteria and material properties of damaged zone were degraded by instantaneous material degradation model. Three geometric degradation models were assumed to estimate the degradation zone around the failure location. The results of two methods were compared with each other. By comparison the results obtained from three degradation models, it was observed that the progressive damage analysis using node degradation model provide marginally better results than two other geometric degradation models, but it takes more time to do computation.

References

Afshin, M. and Taheri-Behrooz, F. (2015), "Interlaminar stresses of laminated composite beams resting on elastic foundation subjected to transverse loading", *Computat. Mater. Sci.*, **96**, 439-447.

Aghaei, M., Forouzan, M.R., Nikforouz, M. and Shahabi, E. (2015), "A study on different failure criteria to predict damage in glass/polyester composite beams under low velocity impact", *Steel Compos. Struct., Int. J.*, **18**(5), 1291-1303.

Argyris, J. and Tenek, L. (1997), "Recent advances in computational thermostructural analysis of composite plates and shells with strong nonlinearities", *Appl. Mech. Rev.*, **50**, 285-306.

Batra, R.C. and Xiao, J. (2013), "Analysis of post-buckling and delamination in laminated composite St. Venant-Kirchhoff beams using CZM and layer-wise TSNDT", *Compos. Struct.*, **105**, 369-384.

Becheri, T., Amara, K., Bouazza, M. and Benseddiq, N. (2016), "Buckling of symmetrically laminated plates using nth-order shear deformation theory with curvature effects", *Steel Compos. Struct., Int. J.*, **21**(6), 1347-1368.

Brubak, L. and Hellesland, J. (2007a), "Approximate buckling strength analysis of arbitrarily stiffened and stepped plates", *Eng. Struct.*, **29**(9), 2321-2333.

Brubak, L. and Hellesland, J. (2007b), "Semi-analytical postbuckling and strength analysis of arbitrarily stiffened plates in local and global bending", *Thin-Wall. Struct.*, **45**(6), 620-633.

Brubak, L. and Hellesland, J. (2008), "Strength criteria in semi-analytical and large deflection analysis of stiffened plates in local and global bending", *Thin-Wall. Struct.*, **46**(12), 1382-1390

Brubak, L., Hellesland, J. and Steen, E. (2007), "Semi-analytical buckling strength analysis of plates with arbitrary stiffener arrangements", *J. Constr. Steel Res.*, **63**(4), 532-543.

Chakraverty, S. and Pradhan, K.K. (2014), "Free vibration of functionally graded thin rectangular plates resting on Winkler elastic foundation with general boundary conditions using Rayleigh-Ritz method", *Int. J. Appl. Mech.*, **6**(4), 1450043.

Fantuzzi, N. and Tornabene, F. (2016), "Strong formulation isogeometric analysis (SFIGA) for laminated composite arbitrarily shaped plates", *Compos. Part B: Eng.*, **96**, 173-203.

Fantuzzi, N., Tornabene, F., Bacciocchi, M. and Ferreira, A.J. (2018), "On the Convergence of Laminated Composite Plates of Arbitrary Shape through Finite Element Models", *J. Compos. Sci.*, **2**(1), 16.

Ghannadpour, S.A.M. and Kiani, P. (2018), "Nonlinear spectral collocation analysis of imperfect functionally graded plates under end-shortening", *Struct. Eng. Mech., Int. J.*, **66**(5), 557-568.

Ghannadpour, S.A.M. and Ovesy, H.R. (2009a), "The application of an exact finite strip to the buckling of symmetrically laminated composite rectangular plates and prismatic plate structures", *Compos. Struct.*, **89**(1), 151-158.

Ghannadpour, S.A.M. and Ovesy, H.R. (2009b), "Exact post-buckling stiffness calculation of box section struts", *Eng. Computat.*, **26**(7), 868-893.

Ghannadpour, S.A.M. and Shakeri, M. (2018), "Energy based collocation method to predict progressive damage behavior of imperfect composite plates under compression", *Latin Am. J. Solids Struct.*, **15**(4), e35.
DOI: https://dx.doi.org/10.1590/1679-78254257

Ghannadpour, S.A.M. and Mehrparvar, M. (2018), "Energy effect removal technique to model circular/elliptical holes in relatively thick composite plates under in-plane compressive load", *Compos. Struct.*, **202**, 1032-1041.

Ghannadpour, S.A.M., Ovesy, H.R. and Zia-Dehkordi, E. (2014), "An exact finite strip for the calculation of initial post-buckling stiffness of shear-deformable composite laminated plates", *Compos. Struct.*, **108**, 504-513.

Ghannadpour, S.A.M., Barvaj, A.K. and Tornabene, F. (2018), "A semi-analytical investigation on geometric nonlinear and progressive damage behavior of relatively thick laminated plates under lateral pressure and end-shortening", *Compos. Struct.*, **194**, 598-610.

Hashin, Z. and Rotem, A. (1973), "A fatigue failure criterion for fiber reinforced materials", *J. Compos. Mater.*, **7**(4), 448-464.

Hayman, B., Berggreen, C., Lundsgaard-Larsen, C., Delarche, A., Toftegaard, H., Dow, R.S., Downes, J., Misirlis, K., Tsouvalis, N. and Douka, C. (2011), "Studies of the buckling of composite plates in compression", *Ships Offshore Struct.*, **6**(1-2), 81-92.

Jiang, G., Li, F. and Zhang, C. (2018), "Postbuckling and nonlinear vibration of composite laminated trapezoidal plates", *Steel Compos. Struct., Int. J.*, **26**(1), 17-29.

Jin, Z-H. and Batra, R.C. (1999), "Thermal shock cracking in a metal-particle-reinforced ceramic matrix composite", *Eng. Fract. Mech.*, **62**, 339-350.

Kamareh, F., Farrokhabadi, A. and Rahimi, G. (2018), "Experimental and numerical investigation of skin/lattice stiffener debonding growth in composite panels under bending loading", *Eng. Fract. Mech.*, **190**, 471-490.

Mahieddinet, A., Ouali, M. and Mazouz, A. (2015), "Modeling and simulation of partially delaminated composite beams", *Steel Compos. Struct., Int. J.*, **18**(5), 1119-1127.

Mehrparvar, M. and Ghannadpour, S.A.M. (2018), "Plate assembly technique for nonlinear analysis of relatively thick functionally graded plates containing rectangular holes subjected to in-plane compressive load", *Compos. Struct.*, **202**, 867-880.

Muthusamy, P. and Sivakumar, S.M. (2014), "A constituent-behavior-motivated model for damage in fiber reinforced

composites", *Computat. Mater. Sci.*, **94**, 163-172.
Naghsh, A., Azhari, M. and Saadatpour, M.M. (2018), "Thermal buckling analysis of point-supported laminated composite plates in unilateral contact", *Appl. Math. Model.*, **56**, 564-583.
Ovesy, H.R. and Ghannadpour, S.A.M. (2011), "An exact finite strip for the nitial postbuckling analysis of channel section struts", *Comput. Struct.* **89**(19), 1785-1796.
Ovesy, H.R., Ghannadpour, S.A.M. and Morada, G. (2005), "Geometric non-linear analysis of composite laminated plates with initial imperfection under end shortening, using two versions of finite strip method", *Compos. Struct.*, **71**(3), 307-314.
Ovesy, H.R., Ghannadpour, S.A.M. and Nassirnia, M. (2015), "Post-buckling analysis of rectangular plates comprising Functionally Graded Strips in thermal environments", *Comput. Struct.*, **147**, 209-215.
Paik, S., Gupta, S.S. and Batra, R.C. (2015), "Localization of buckling modes in plates and laminates", *Compos. Struct.*, **120**, 79-89.
Patel, S.N. (2014), "Nonlinear bending analysis of laminated composite stiffened plates", *Steel Compos. Struct., Int. J.*, **17**(6), 867-890.
Su, Z.C., Tay, T.E., Ridha, M. and Chen, B.Y. (2015), "Progressive damage modeling of open-hole composite laminates under compression", *Compos. Struct.*, **122**, 507-517.
Sun, Y., Li, S.R. and Batra, R.C. (2016), "Thermal buckling and post-buckling of FGM Timoshenko beams on nonlinear elastic foundation", *J. Thermal Stress.*, **39**(1), 11-26.
Topal, U. (2013), "Application of a new extended layerwise approach to thermal buckling load optimization of laminated composite plates", *Steel Compos. Struct., Int. J.*, **14**(3), 283-293.
Tornabene, F., Fantuzzi, N. and Bacciocchi, M. (2017), "Linear static behavior of damaged laminated composite plates and shells", *Materials*, **10**(7), 811, 1-52.
Tornabene, F., Fantuzzi, N., Bacciocchi, M. and Viola, E. (2018), "Mechanical behavior of damaged laminated composites plates and shells: higher-order shear deformation theories", *Compos. Struct.*, **189**, 304-329.
Vedrtnam, A. and Pawar, S.J. (2017), "Laminated Plate Theories and Fracture of Laminated Glass Plate-A Review", *Eng. Fract. Mech.*, **186**, 316-330 .
Vu, T.V., Khosravifard, A., Hematiyan, M.R. and Bui, T.Q. (2018), "A new refined simple TSDT-based effective meshfree method for analysis of through-thickness FG plates", *Appl. Math. Model.*, **57**, 514-534.
Yang, Q.J. and Hayman, B. (2015a), "Prediction of post-buckling and ultimate compressive strength of composite plates by semi-analytical methods", *Eng. Struct.*, **84**, 42-53.
Yang, Q.J. and Hayman, B. (2015b), "Simplified ultimate strength analysis of compressed composite plates with linear material degradation", *Compos. Part B: Eng.*, **69**, 13-21.
Yang, Q.J., Hayman, B. and Osnes, H. (2013), "Simplified buckling and ultimate strength analysis of composite plates in compression", *Compos. Part B: Eng.*, **54**, 343-352.
Zhang, Y.X. and Yang, C.H. (2009), "Recent developments in finite element analysis for laminated composite plates", *Compos. Struct.*, **88**(1), 147-157.